Investigating Aerodynamic Coefficients and Stability Derivatives for Truss-Braced Wing Aircraft Using OpenVSP

Varun S. Sarode

Thesis submitted to the Faculty of the

Virginia Polytechnic Institute and State University

in partial fulfillment of the requirements for the degree of

Master of Science

in

Aerospace Engineering

Rakesh K. Kapania, Chair

Joseph A. Schetz

Pradeep Raj

February 21, 2022

Blacksburg, Virginia

Keywords: Aerodynamics, Truss-Braced Wing, OpenVSP, Flight Dynamics, Stability Derivatives

Investigating Aerodynamic Coefficients and Stability Derivatives for Truss-Braced Wing Aircraft Using OpenVSP

Varun S. Sarode

ABSTRACT

As the necessity of sustainable mobility rises, the demand to reduce the environmental impact of transporting mediums increases. The SUGAR Truss-Braced Wing (TBW) aircraft is a venture of Boeing, NASA and Virginia Tech for the N+3 generation of aircraft. These high-aspect-ratio aircraft are being designed with the aim to improve the structural and aerodynamic performance by implementing advanced technologies. Aerodynamics is a major factor influencing the performance of the aircraft, affecting the fuel consumption and emissions, especially due to drag. The multidisciplinary design optimization architecture for truss-braced-wing aircraft is dedicated to generate configurations with low fuel burn, maximum weight carrying capabilities and aircraft stability for long and medium range missions. The incorporation of flight dynamics at the conceptual design stage offers enhanced aerodynamic performance and wing flexibility for the aircraft. A robust flight dynamic system would need a detailed aerodynamic analysis of the aircraft with the focus on aeroelasticity. In this thesis, various aerodynamic coefficients and stability derivatives are investigated by applying Vortex-Lattice Method using OpenVSP, an open-source platform. The variation in aerodynamic parameters with changes in configurations and flow conditions are discussed as well. OpenVSP allows for study of these results with low computational expense. This will aid in efficient aerodynamic design and lay basis for flight dynamics analysis and its inclusion in the Multidisciplinary Design Analysis and Optimization (MDAO) framework.

Investigating Aerodynamic Coefficients and Stability Derivatives for Truss-Braced Wing Aircraft Using OpenVSP

Varun S. Sarode

GENERAL AUDIENCE ABSTRACT

The demand for sustainable mobility and green transportation is increasing. Reduction in the environmental impact of these mediums is the prime motivation for various research studies conducted in this domain. The SUGAR Truss-Braced Wing (TBW) aircraft configuration research, led by Boeing, NASA and Virginia Tech over the last two decades, aims at developing highly fuel-efficient next-generation aircraft. These high-aspect-ratio aircraft are being researched for improving the structural and aerodynamic performance by implementing advanced technologies. Aerodynamic performance of the aircraft influences the fuel consumption and emissions produced drastically. The current design optimization framework for the TBW aircraft focuses on development of these aircraft configurations with the goal to limit fuel burn and maximize payload carrying capability. Flight dynamics analysis can be significant to improve and obtain optimal solutions from the design process. Incorporation of flight dynamics at the conceptual design stage offers enhanced aerodynamic performance and wing flexibility for the next generation aircraft. Therefore, a detailed aerodynamic analysis of the aircraft would be needed to establish a systematic flight dynamics module. This thesis presents a new approach for formulating and analysing the aerodynamic coefficients and stability derivatives by implementing Vortex-Lattice Method available in the open-source software. This will further allow for inclusion of flight dynamics study of the new configurations for long and medium range missions within the existing framework.

Dedicated to my family and close friends

Acknowledgments

I would like to start with the most sincere acknowledgement towards my advisor Dr. Rakesh K. Kapania for providing me with the platform and opportunity to explore the domain of aircraft design. He has been a constant source of motivation and guidance throughout my journey at Virginia Tech. He has given the necessary financial and moral support and has been extremely patient with my progress through the course.

I take the opportunity to extend my earnest acknowledgements to Dr. Joseph A. Schetz for helping with his valuable experience and support. Dr. Schetz has dedicated detailed attention to the progress of my research and his feedback has been very crucial. He has also shown great understanding and patience with my development. Their technical suggestions and comments have groomed me both academically and professionally.

I would also like to express my gratitude to Dr. Rikin Gupta, a former Ph.D. student of Dr. Kapania's group for directing me to this particular section of research and demonstrating the potential for flight dynamics of TBW aircraft. He helped me a lot in my starting phase with the research group and has shown great support even after his graduation. I would like to thank Varakini Sanmugadas, a Ph.D. candidate, for helping with multiple concepts and understanding the MDAO architecture for the group. Furthermore, I would thank Kamrul H. Khan, another Ph.D. candidate within the TBW research group. His initial help with understanding the ModelCenter framework and development of the parallel processing framework has been helpful to my work.

My parents and sister have been a backbone for me throughout my life, I am thankful for having been blessed with such a family and my extended family. Their belief in me and their determination to push me up has made me who I am right now.

I would like to thank my colleagues in Blacksburg, my roommate and my loved ones, without whom this journey at Virginia Tech would seem impossible, especially during unprecedented times of the pandemic. I am grateful for their presence and help with almost everything within and outside the graduate school.

I would also thank Virginia Tech and the Department of Aerospace Engineering, along with Dr. Stefano Brizzolara, for giving me the opportunities and resources to pursue my dream of an Aerospace Engineering graduate.

Contents

List of Figures

List of Tables

List of Abbreviations

α	Angle of attack, deg
β	Angle of sideslip, deg
Γ	Vortex Strength, per unit length
b	Span of a lifting surface, ft
c	Mean chord length, ft
C_D	Three-dimensional drag coefficient
c_d	Local drag coefficient
C_L	Three-dimensional lift coefficient
c_l	Local lift coefficient
C_M	Aerodynamic pitching-moment coefficient
C_N	Aerodynamic yawing-moment coefficient
c_p	Pressure coefficient
C_S	Aerodynamic side-force coefficient
C_{D_i}	Induced drag coefficient
C_{D_p}	Parasite drag coefficient
C_{D_w}	Wave drag coefficient

$C_{L_{roll}}$ Aerodynamic rolling-moment coefficient

L/D Lift-to-Drag ratio

M_∞ Mach Number

P Role rate, rad/s

Q Pitch rate, rad/s

R Yaw Rate, rad/s

Re Reynolds Number

S Reference Surface Area, ft^2

t/c Thickness-to-Chord ratio

u Surge Velocity, ft/sec

V_∞ Reference Freestream Velocity, ft/sec

Chapter 1

Introduction

1.1 Background and Motivation

Aircraft research has become very intensive over the last few decades with the goal to improve efficiency, due to limited natural resources and rise in fuel costs. This has led to initiation of several research programs for minimizing the fuel consumption of aircraft. The commercial and transport aircraft industry is a major consumer of these resources. According to the United States Department of Transportation, the annual fuel consumption has increased by 12.05% between 2010-2019 [6]. The annual fuel consumption for 2019 was 18.27 billion gallons, which suggests that a small percentage reduction in an aircraft's fuel burn, would save millions of gallons and reduce the corresponding emissions. The tube and wing aircraft configuration has been dominantly used for commercial planes and jet planes over last several years. Many advanced technologies have been implemented to improve the fuel efficiency of these planes. Aerodynamics significantly affect the fuel consumption of an aircraft, and despite the technological developments, substantial aerodynamic performance improvements are limited with this configuration. It is a matter of course, that new wings and configurations are explored to overcome such limitations. These configurations are needed to have high flexibility and should be studied extensively before they can be taken further into application. The continuous development in the analysis and simulation capabilities allows for such comprehensive research.

Werner Pfenninger [1] first visualized the strut-braced wing (SBW) and truss-braced wing (TBW) configurations for modern transport aircraft. The SBW configuration has an additional member (strut) connecting the main wing to the fuselage, and the TBW uses additional truss member to connect the main wing to the strut. Pfenninger's proposed design for the Truss-braced wing configuration in the 1970s is as shown in Figure 1.1. The detailed schematics are discussed later in the work.

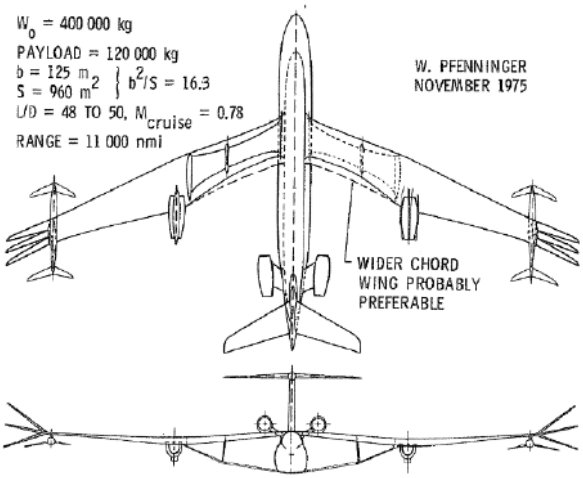

Figure 1.1: Pfenninger's [1] vision of TBW configuration.

The Virginia Tech Multidisciplinary Design Optimization architecture [7, 8, 9] for transonic aircraft is based on this version of the truss-brace wing configuration. The additional strut and truss members stiffen the wing structure. These members help in reducing the spanwise bending moment, which reduces the t/c for the main wing along with the reduced chord length. This minimizes the skin thickness as well. A combination of these reductions leads to a decrease in the Reynolds number. The stiffening of the wing structure due to members, allows for larger span, thereby, increasing the aspect ratio. A reduced airfoil thickness and a higher aspect ratio decreases the form and wave drag and induced drag, respectively. Low

Reynolds number and less span-wise cross flow due to unsweeping of wings, combine to allow an increased laminar flow [10], which is desirable.

These structural and aerodynamic benefits collaborate to lower the structural weight, improve the aerodynamic performance by reducing drag and eventually reduce fuel consumption. The benefits and challenges for these configurations have been discussed in previous studies extensively [9, 11, 12, 13]. This is the overall motivation behind pursuing the TBW and SBW configurations.

The incorporation of flight dynamics at the conceptual design stage offers enhanced aerodynamic performance and wing flexibility for such aircraft. Gupta et al. [14] studied the development of an analysis framework establishing that incorporating flight dynamics modeling into the MDAO process is useful in optimizing vehicle designs for flexible aircraft. A robust flight dynamic system would need a detailed aerodynamic analysis of the aircraft with focus on aeroservoelasticity. This is the motivation to study the aerodynamic coefficients and stability derivatives for these aircraft configurations. OpenVSP [15] provides the user the possibility to create three-dimensional models of aircraft and perform engineering and aerodynamic analyses on those models. VSPAero is a tool within the VSP environment that allows for such aerodynamic analysis using Vortex-Lattice Method (VLM) or panel method. The current study is based on using VLM for investigating these aerodynamic parameters.

1.2 Current Architecture and Related Work

The VT MDO framework can use three types of configurations to perform the design optimization. Those are cantilever, SBW (Strut-braced wing) and TBW (Truss-braced wing). A simple layout of the SBW wing can be seen in Figure 1.2. There is a strut that connects the high wing to the fuselage.

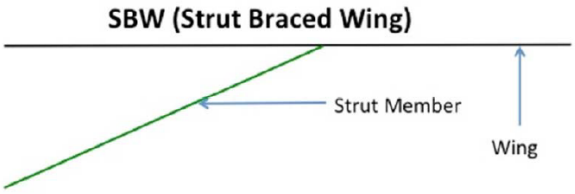

Figure 1.2: SBW Configuration basic sketch.

In the case of the TBW configuration, an additional jury member is connected. As shown in Figure 1.3, this member provides additional support to the wing. Thus, the bending stress is reduced. The other advantage, is that it allows for shorter effective length of the strut, which helps in minimizing the possibility of the strut buckling under negative load factors. The downside to adding this member is that it generates additional interference drag and adds to the aircraft weight.

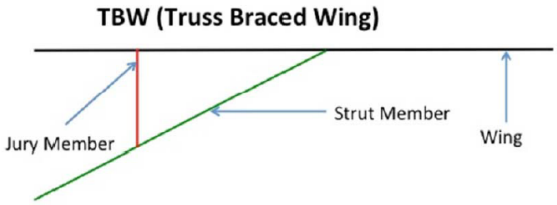

Figure 1.3: TBW Configuration basic sketch.

The MDAO framework used for TBW study at Virginia Tech has been based in the integration and optimization software ModelCenter [16]. This system allows for complete integration of various in-house analysis codes and packages into an enclosed environment. The software program has multiple analysis and optimization nodes interconnected via links. These analysis codes have been developed using Fortran and C++. Python packages called

Wrappers are used to connect these codes to different analysis nodes. The detailed manual explains the ModelCenter environment and its application for the aircraft optimization which is shown in Figure 1.4. The previous TBW studies have used this package over the last several years.

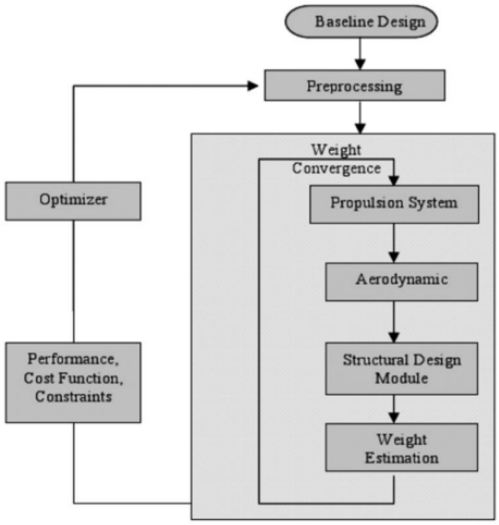

Figure 1.4: The MDO framework for TBW study [2]

Recently, Khan et al. carried out a study for VT MDO [17] for developing DELWARX, a python based framework, for multidisciplinary design optimization of TBW aircraft. This framework used similar packages and codes developed in previous MDO studies but compiled in Linux operating system. This overcomes the system and memory-related issues with the operating systems. This framework also allows for parallel optimization which leads to a significant reduction in the computing time. This was limited by sequential programming in the previous framework. The flight dynamics framework is to be included evetually within this architecture of parallel optimization.

This study is conducted with the aim to obtain the preliminary aerodynamic data. TBW configurations at Mach 0.7 and Mach 0.8 are analysed for current market single-aisle config-

urations aircraft mission with a passenger capacity of around 200 and a range of 3500NM, similar to profile in a previous study [2]. In this thesis, a potential flow method (VLM) has been implemented using an open source package. Parameters such as lift, drag, local coefficients and variation in these parameters have been analysed. Coefficients, derivatives and stability derivatives have been presented as well for different configurations.

Chapters 1 and 2 discuss the related work and current framework from the literature. The modeling of different configurations with varying geometry is presented in Chapter 3. Further, Chapter 4 discusses the background on Vortex-lattice method, and its implementation through VSPAero. The flow conditions and VLM geometry are illustrated as well. Chapter 5 presents the output and results obtained for different configurations. It presents variation in aircraft aerodynamics with variation geometry, flow conditions and stability parameters. The comparison between coefficients and derivatives at a particular angle of attack and Mach number has been illustrated for three different configurations. Chapter 5 also discusses additional considerations needed to account for non-linearities in the flow for this application. The last chapter discusses the summary of the study and the scope for future work. It presents the utility and potential of the OpenVSP package for inexpensive aerodynamic analyses.

Chapter 2

Literature Review

The TBW configuration has been studied extensively to understand and improve its structural and aerodynamic capabilities. Studies [18, 19] conducted during the start of the 21st century, investigated and demonstrated the advantages of a strut-braced wing. The results of which were compared to cantilever wing configurations (tube and wing). The results were able to show that this configuration could potentially minimize take-off gross weight (TOGW), improve fuel consumption and operate for long-range transports, encouraging the focus on braced-wing configurations.

The VT MDO group performed a detailed study to analyse the potential and challenges of TBW configurations [7]. The truss structure allows for larger wing spans. NASTRAN based analysis is performed on the two configurations. Larger wing spans tend to decrease the natural frequencies of the wing structure and influences the flutter characteristics. The development of the existing VT MDO framework was carried out in studies [9, 11] using various software packages and modules. This framework has continued to carry out different design and optimization analysis for TBW configurations for medium and long range missions. It used a set of design variables and constraints to obtain the optimal design solution for the aircraft. Based on this framework, various studies were conducted by the Virginia Tech MDO research group to investigate the advantages of SBW and TBW wing configurations over conventional cantilever wing aircraft. The underlying objective for these optimizations was to minimize the TOGW and reduce the fuel consumption of the aircraft [12, 13, 20].

Furthermore, studies were conducted to see the effect of flutter and transonic aeroelasticity with the goal to integrate linearized unsteady aeroelastic analysis in the MDO framework [10, 21].

Including flight dynamics at the conceptual stage would further enhance the optimization capabilities of the existing architecture. This will also allow for improving the controllability of the aircraft. The mAEwing optimization framework developed at VT has incorporated the flight dynamic model within the MDAO process [14, 22]. This research clearly illustrates simultaneously satisfying two objectives of weight minimization and control maximization for optimal designs. These investigations show that inclusion of flight dynamics within the TBW will improve the design process. Investigating the transonic effects for transport aircraft, using computationally inexpensive tool like VLM has been demonstrated in research by NASA Ames Center [5]. Another study for developing integrated Nonlinear Aeroservoelastic Flight Dynamic Model [23] has been conducted for TBW in 2017. It uses the VORLAX VLM aerodynamic model. FEM is utilized in order to create a notional structural model of the TBW utilizing equivalent beams for the wing and the main strut. Longitudinal response for linearized and nonlinear models are shown.

Another study by Ting et al. [3] implements aerodynamic superposition approach to deal with the complexity of the TBW configuration. This study uses VORLAX VLM for aerodynamic analysis of the TBW aircraft. The results from two different superposition approaches are then compared to those obtained from the CFD codes- USM3D and FUN3D. Figure 2.1 and Figure 2.2 show the two methods of superposition implemented in the research. This study does not consider the jury as a lifting surface. These figures demonstrate the application of the superposition by summation and subtraction for the components while using the superposition approach. The first approach sums the fuselage-wing-tail combination and the fuselage-strut-tail combination, and then subtracts the fuselage-tail component contribu-

tion. The second approach is just summation of all the different components' contribution. The results from this superposition method show good agreement with the results in CFD computed using the methods mentioned earlier.

Figure 2.1: Aerodynamic Superposition Method 1 for TBW Model [3]

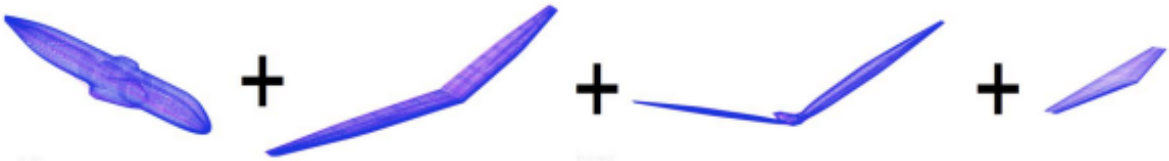

Figure 2.2: Aerodynamic Superposition Method 2 for TBW Model [3]

The present study aims to leverage the utility of the VSP package to compute similar results. The approach can help eliminate the post processing of results and provides a appropriate analysis for the aircraft aerodynamics. The VSPAero module also provides a dynamic and user-friendly interface to investigate varying parameters and trends. This will allow for further ease in incorporating the flight dynamics within the framework. The open-source platform has great compatibility with different software package systems such as NASTRAN, MATLAB and CAD modeling tools, which aids in flexible use of the program.

Chapter 3

Modeling of the configurations in OpenVSP

OpenVSP is an abbreviation of Open Vehicle Sketch Pad [15]. Initially developed by NASA, it provides an open source tool for parametric aircraft geometry. With several developments in the software package, it allows for generating three-dimensional aircraft models and performing a detailed aerodynamic analysis and a primary structural analysis on these models. VSPAero uses these models to generate the required analysis. For conducting the aerodynamic analysis, a three-dimensional model is generated within the VSP module. The geometric parameters are defined to generate different aircraft components like wing, pod, fuselage, propellers, tails, etc.

3.1 Model Descriptions and Geometric Parameters

For generating the VLM geometry, a 3-D model of the four configurations are created in the sketch pad. The geometric data is formulated based on the models employed in the previous studies [11, 12, 21, 24]. The cantilever configuration has a span of 169.62 ft. It has a conventional tube and wing structure, with rest of the parameters same as that of SBW configuration. Figure 3.1 shows the isometric view for the SBW configuration. The fuselage, the strut, the horizontal and vertical tails are modeled along with the main wing.

The aspect ratio for this particular configuration is 18.11. The geometric information such as span, aspect ratio, root chord length of the wing and the strut are given in Table 3.1.

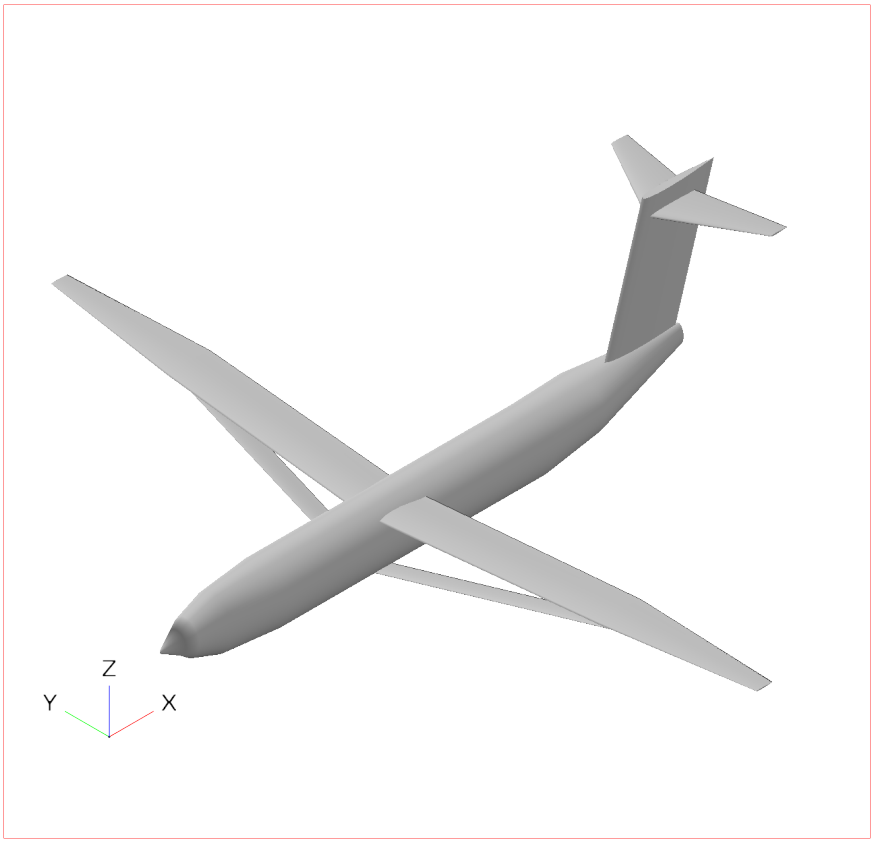

Figure 3.1: SBW configuration- Isometric view

Table 3.1: SBW aircraft configuration parameters

Wing	Span	Aspect Ratio	Area	Root Chord	Taper Ratio
Main	169.62 ft	18.11	1588.79 ft^2	11.16 ft	0.354
Strut	104.85 ft	24.54	448.09 ft^2	4.27 ft	1

Figure 3.2 shows the front and top views of the configuration. It can be seen that the strut is connected to the main wing by an extending vertical member.

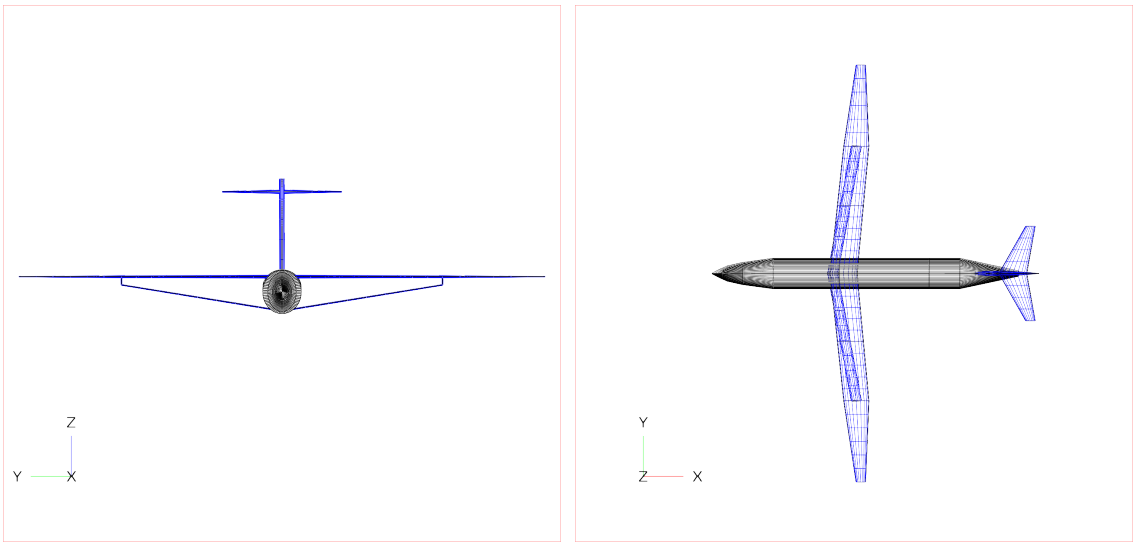

(a) (b)

Figure 3.2: SBW Configuration- (a) Front View and (b) Top View

The TBW configuration is based on the geometric data available from previous studies for MDO and aerodynamic analysis [2, 9, 21, 24]. The additional jury member added between the strut and main wing, provided added strength to the wing allowing reduced t/c. The aspect ratio for the main wing for this configuration is similar to the one for the SBW, although this configuration can allow for higher aspect ratios given the improved wing structure. Figure 3.3 shows the isometric view of the TBW configuration. The data associated with the aircraft parameters is represented in Table 3.2.

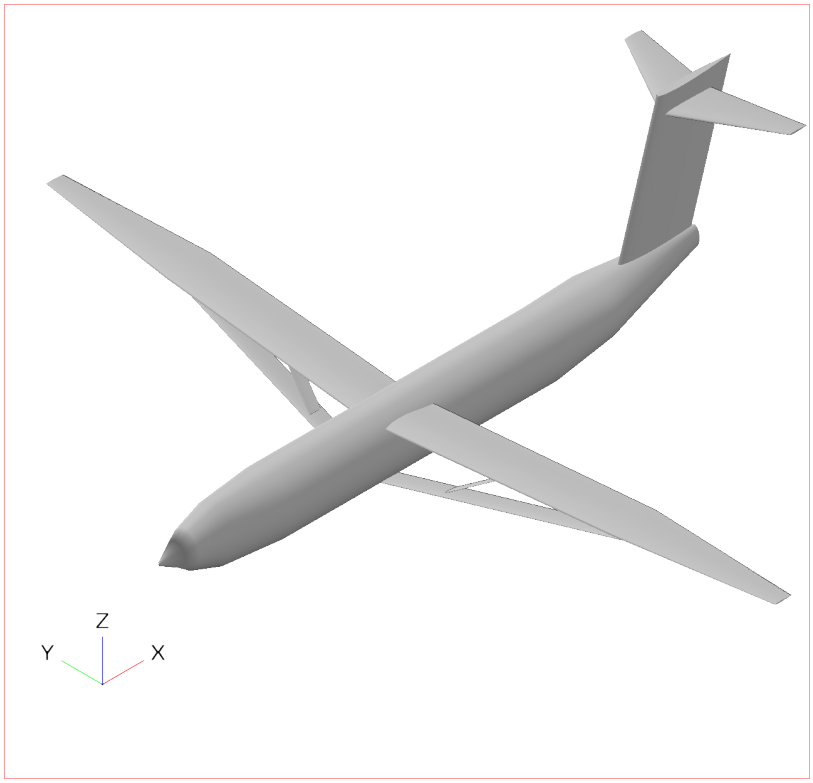

Figure 3.3: TBW configuration- Isometric view

Table 3.2: TBW aircraft configuration parameters

Wing	Span	Aspect Ratio	Area	Root Chord	Taper Ratio
Main	169.62 ft	18.11	1588.79 ft^2	11.16 ft	0.354
Strut	104.85 ft	24.54	448.09 ft^2	4.28 ft	1
Truss	27 ft	10.58	72.23 ft^2	2.61 ft	1

Figure 3.4 shows the front and top views of the TBW configuration, displaying the location of the strut and the jury.

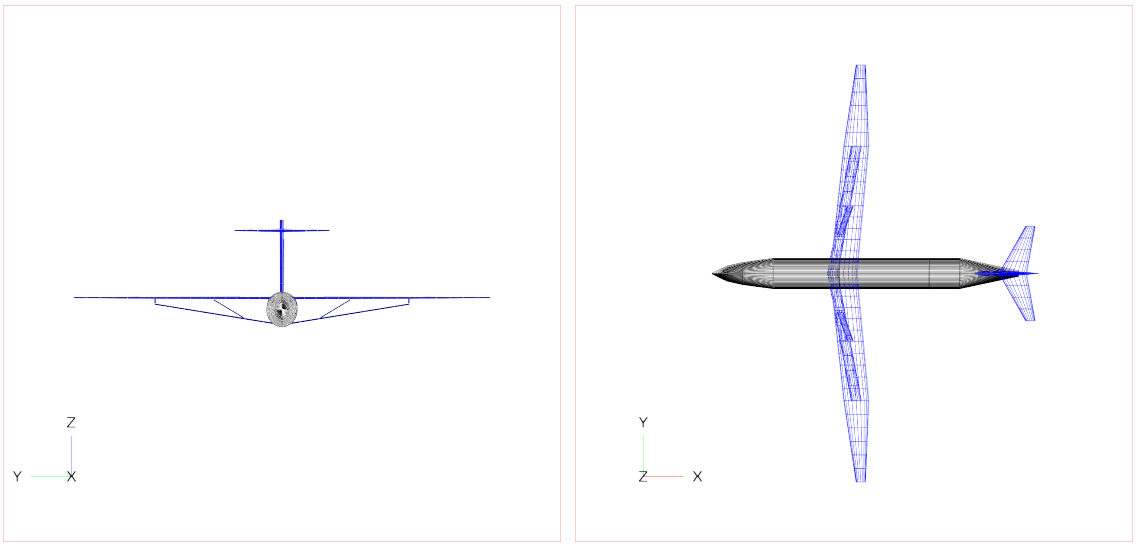

(a) (b)

Figure 3.4: TBW Configuration- (a) Front View and (b) Top View

Additionally, a new TBW configuration is considered with a higher aspect ratio. The main wing span for TBW-II configuration is 189.62 ft. Table 3.3 displays the detailed geometric parameters for the main wing, the modified strut and jury member for TBW-II configuration. Figure 3.5 shows the isometric view of this new configuration.

Table 3.3: TBW-II aircraft configuration parameters

Wing	Span	Aspect Ratio	Area	Root Chord	Taper Ratio
Main	189.62 ft	20.24	1776.125 ft^2	11.16 ft	0.354
Strut	116.93 ft	27.36	499.64 ft^2	4.28 ft	1
Truss	31.53 ft	12.07	82.40 ft^2	2.61 ft	1

Figure 3.6 shows the front and top views of the TBW configuration, displaying the location of strut and jury members.

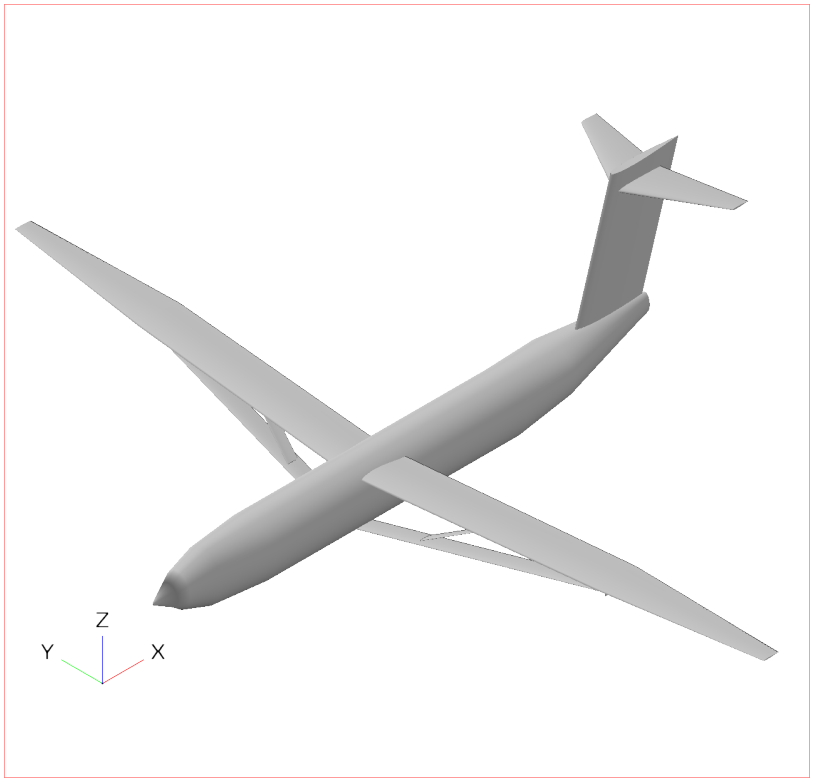

Figure 3.5: TBW-II configuration- Isometric view

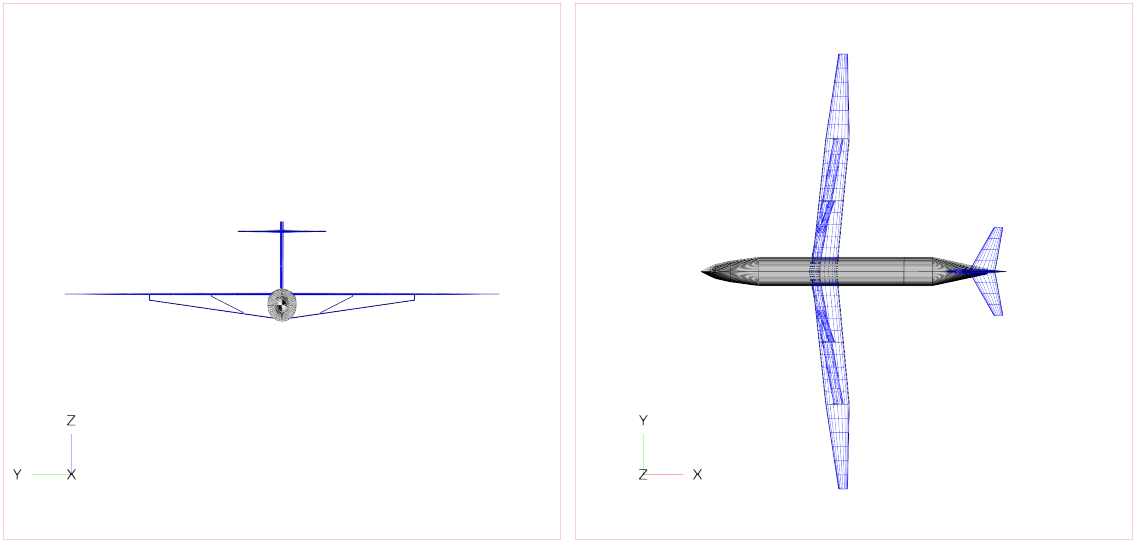

(a) (b)

Figure 3.6: TBW-II Configuration- (a) Front View and (b) Top View

3.2 VLM Based Aerodynamic Models

A vortex-lattice method (VLM) based model gives three-dimensional wing aerodynamic solution of any general form. For an incompressible, inviscid flow, a set of lifting panels is used for modeling a wing. These panels have a horse-shoe vortex in each one of them. A bound vortex is situated at 1/4th chord position on the panel and two trailing lines of vortex being shed from each end as shown in Figure 3.7. A surface flow boundary condition is applied on each panel to calculate the required strength of the bound vortex for every panel [25]. The condition of no flow normal to the surface is applied, see equation 3.1, where w is panel inflow velocity and θ is pitch.

$$V_n = 0 = V_\infty \sin(\theta_i) + w_i \tag{3.1}$$

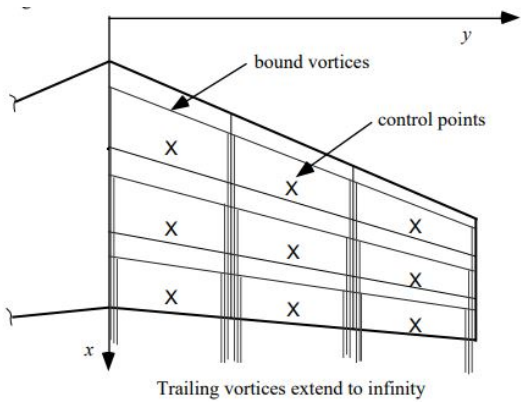

Figure 3.7: Horseshoe Vortex representation on a lifting panel on the wing [4]

The aforementioned no-flow condition is applied at 3/4th chord position along the panel's mid-span. The freestream component in the normal direction and the induced flow component together make up the the normal velocity. The induced component is derived from

the strength of all vortex panels of the wing. Thus, a linear combination of the effects of the strengths of all panels on the induced velocity is set up as one equation for every panel, see equation 3.2. A matrix of influence coefficients is formulated and it is multiplied by the vector of vortex strengths of all vortices and this is equated to a vector representing the freestream effects.

$$w_i = \sum_{j=1}^{j=N} A_{ij}\Gamma_j \tag{3.2}$$

$$\sum_{j=1}^{j=N} A_{ij}\Gamma_j = -V_\infty \sin(\theta_i) \approx -V_\infty \theta_i \tag{3.3}$$

The influence coefficient A_{ij} represents the induced flow on panel i due to the vortex on panel j. Γ_j is the vortex strength of panel j. If all panels are assumed to be approximately planar then this influence coefficient can be calculated as a relatively simple application of the Biot-Savart law along the three component vortex lines as,

$$w_{ij} = \frac{\Gamma_j}{4\pi} f(r_{ij}) \tag{3.4}$$

In matrix form, this equation becomes

$$w = A\Gamma \tag{3.5}$$

The panel inflow velocity w_i is defined as the velocity at the panel control point which is located at the mid span and mid chord of the panel. Each panel has two degrees of freedom i.e., heave (Z) and pitch (θ). Then the w_i vector can be written as,

$$w_{\infty i} = w_{\infty i\theta} + w_{\infty i\dot{Z}} + w_{\infty i\dot{\theta}} \tag{3.6}$$

$$w_{\infty i\theta} = -V_\infty \sin\theta_i \approx -V_\infty \theta_i \qquad w_{\infty i\dot{Z}} = \dot{Z}_i \qquad w_{\infty i\dot{\theta}} = \frac{-c_i}{4}\theta_i \tag{3.7}$$

The lift coefficient for the wing at a given angle of attack will be obtained by summing the lift on each panel. The lift on a particular panel can be found using the Kutta relation:

$$L_i = \rho_\infty V_\infty \Gamma_i b_i \tag{3.8}$$

$$L_i = \rho_\infty \Gamma_i |V_\infty i| L_i \sin(\psi_i) \tag{3.9}$$

The equation can be written in the matrix form as,

$$L = \rho_\infty L' \hat{V}_p \Gamma \tag{3.10}$$

After the three-dimensional geometry model has been defined, the VLM geometry is formulated in the VSP environment. This is generated by the choosing the *DegenGeom* command under the *Analysis* tab. The next step is to define various inputs and the flow conditions. The overall process of VSPAero modeling and configuration is shown in Figure 3.8. The details for the modeling process and the VSP GUI can be found in Appendix A.

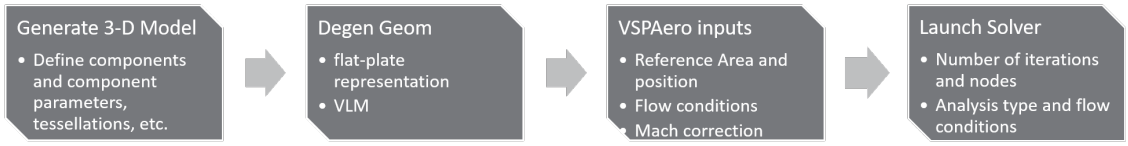

Figure 3.8: Flow of VSPAero modeling and configuration

The fuselage is modelled as a non-lifting surface in VSPAero. Thus, there is no lift or induced drag accounted from it. However, the lift on the strut and jury members is considered

in the current model. Figure 3.9 shows the VLM geometry setup for the cantilever wing configuration.

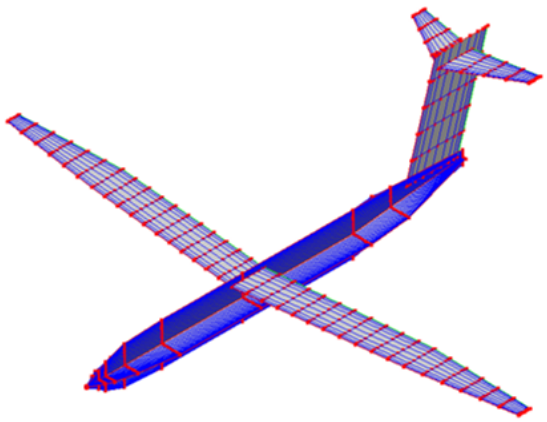

Figure 3.9: VLM geometry visualization for Cantilever Wing configuration

The three-dimensional model is discretized into sections along the span and chord within the modeling setup of OpenVSP. The *DegenGeom* function converts this model into a flat plate representation of the geometry. The discretization of the fuselage, wing and other lifting components into a series of flat panels can be seen in these figures. The user can define the number of tessellations in each direction for every component in the 3-D model, more details and procedure for VSPAero modeling can be found in the forum [26]. VSPAero allows for clustering tessellations. The leading and trailing edge have additional panels to appropriately capture aerodynamic variations in the region. Figure 3.10 and Figure 3.11 show the VLM geometry setup for the SBW and TBW configurations, respectively for reference.

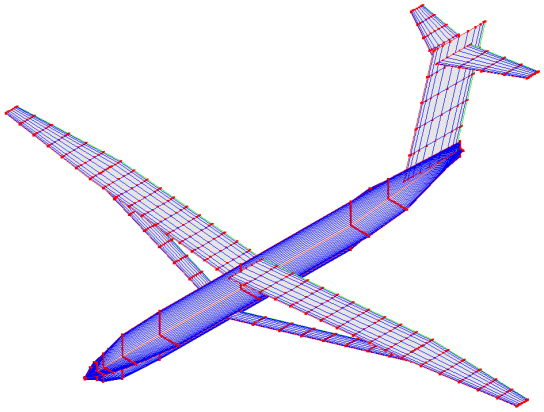

Figure 3.10: VLM geometry visualization for SBW configuration

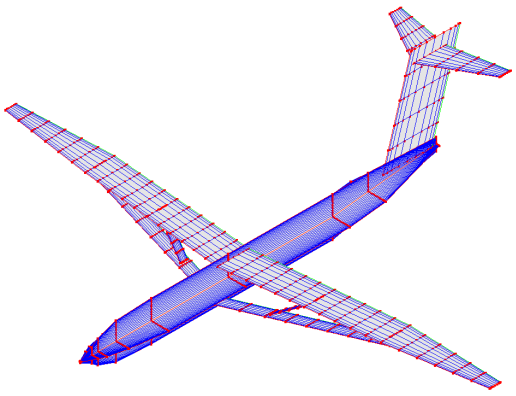

Figure 3.11: VLM geometry visualization for TBW configuration

Mach correction is required for considering the compressibility effect for the aircraft application. This can be done by using Prandtl-Glauret rule or the 2^{nd} Order Karman-Tsien Rule. VSPAero allows for use of the Karman-Tsien Rule, which can be explained by the following approximate equation that allows the pressure coefficient, c_p, for a compressible subsonic flow to be obtained from the value for incompressible flow, c_{p_i}, according to equation,

$$c_p = \frac{c_{p_i}}{\sqrt{1 - M_\infty^2} + \frac{M_\infty^2}{1+\sqrt{1-M_\infty^2}} \frac{c_{p_i}}{2}} \tag{3.11}$$

The total drag consists of three main components, such as Induced Drag (C_{D_i}), Parasite Drag (C_{D_p}) and wave drag (C_{D_w}). For this study, VSPAero only accounts for induced drag and skin friction drag, which is part of the parasite drag. The wave drag is not considered here. An external package will be needed to model wave deag.

The additional details about the setup of VSPAero for the analysis can be found in Appendix A.

Chapter 4

Results and Discussion

This chapter discusses the results generated by implementing the VLM through the VSPAero module and studying the lift and drag distributions for different configurations. It is important to look at the computation time taken for analyzing these configurations with regards to complexity of the geometry. The variation in lift, drag and local aerodynamic coefficients at different angles of attack and different Mach numbers gives an overview of the deviation in aerodynamic characteristics with changes in flow conditions. The VSPAero module also gives the convergence history for these analyses with respect to number of iterations. After studying this convergence history for different simulations, a fixed number of iterations has been adopted for all the following cases. The aerodynamic coefficients and the stability derivatives obtained from the module have been presented as well. Four cases have been presented here with different configurations such as Cantilever, SBW, TBW-I and TBW-II. These configurations are studied at an angle of attack of 2, 2.5 and 3 deg, and corresponding Mach number of 0.7 and 0.8. A steady analysis type with variation in P, Q and R, along with Mach number and surge velocity is conducted.

4.1 Aerodynamic Results for Cantilever Wing Configuration from VSPAero

The results for the cantilever wing configuration, a conventional (tube and wing), Figure 3.9, are presented in this section. The convergence history for the lift coefficient and drag coefficient is illustrated in Figure 4.1, and 4.2, respectively. The lift coefficient for Mach number 0.7 and 0.8 varies between 0.32 to 0.61 at different angles of attack. The case of angle of attack of 2 deg and Mach number of 0.8 generate an approximately identical lift coefficient for the case of angle of attack 2.5 deg and Mach number of 0.7. Similar trend is observed for the drag coefficient and lift-over-drag ratio, the convergence history for which is presented in Figure 4.3.

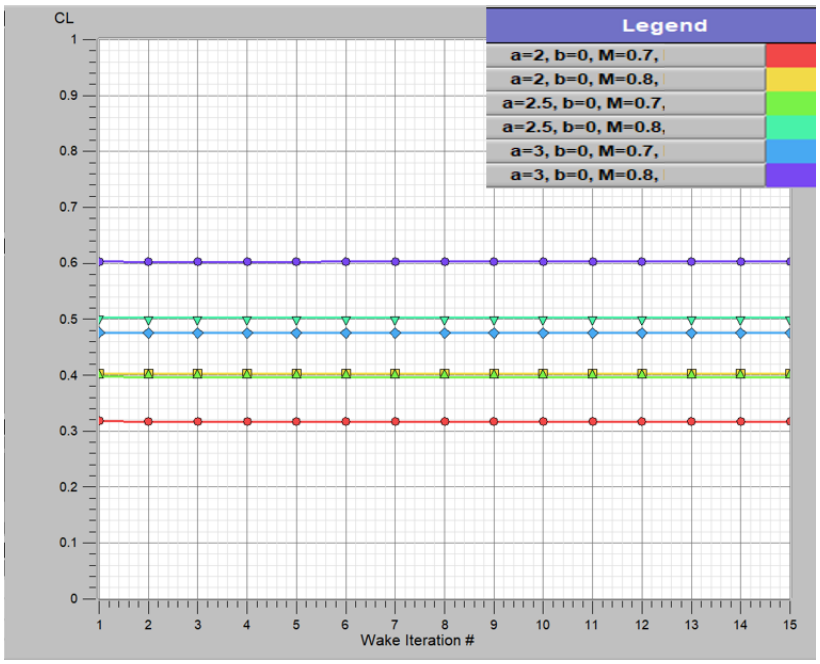

Figure 4.1: Convergence of C_L for α=2, 2.5 and 3 deg at M_∞=0.7 and 0.8 -CANW

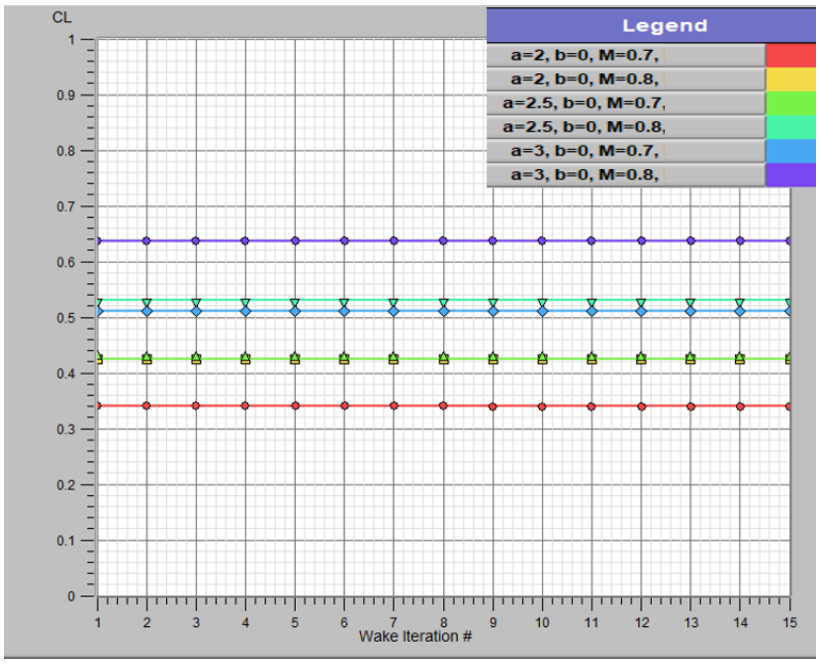

Figure 4.2: Convergence of C_D for α=2, 2.5 and 3 deg at M_∞=0.7 and 0.8 -CANW

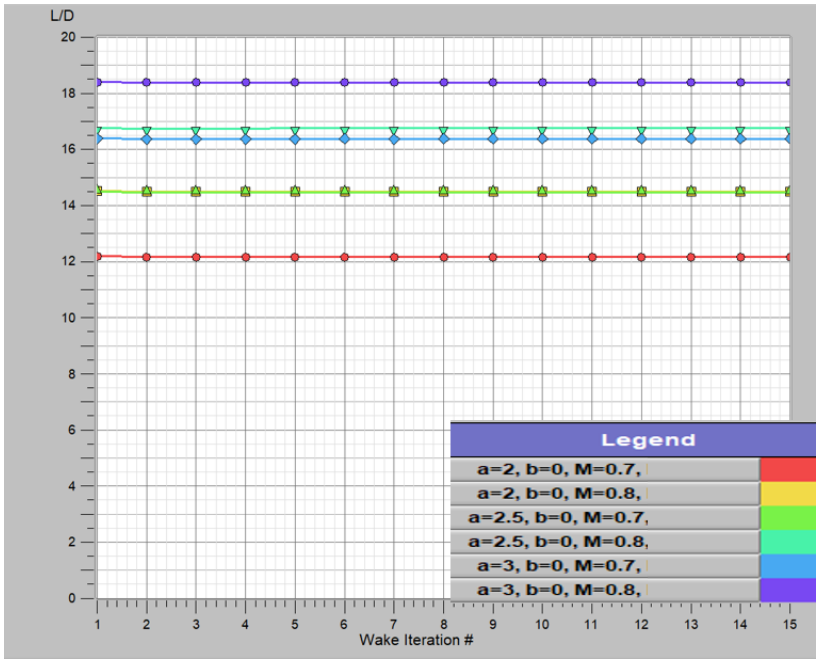

Figure 4.3: Convergence of L/D for α=2, 2.5 and 3 deg at M_∞=0.7 and 0.8 -CANW

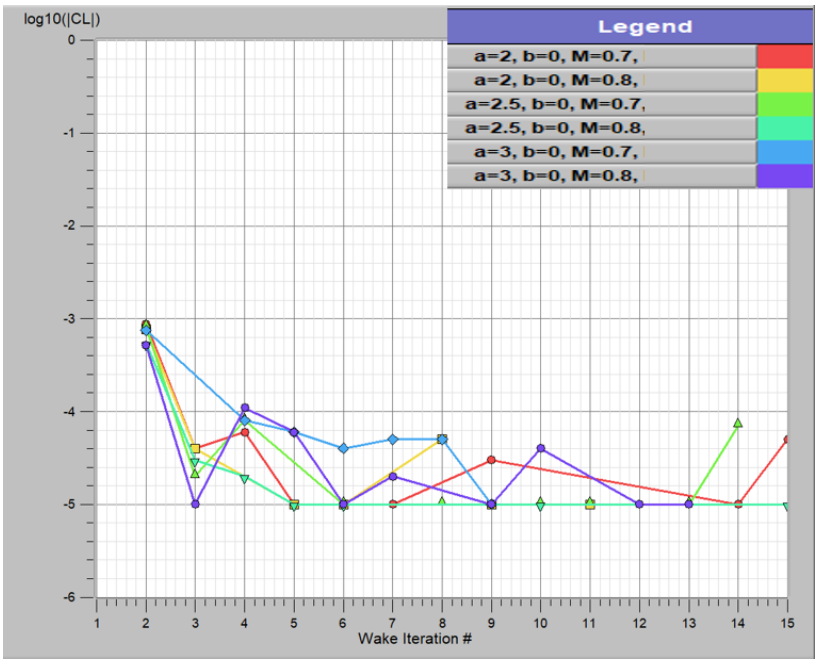

Figure 4.4: Residual for C_L for α=2, 2.5 and 3 deg at M_∞=0.7 and 0.8 -CANW

The residual history for this configuration is shown in Figure 4.4. The computation time for this configuration is 6900.58 sec. A Department of Aerospace and Ocean Engineering, Virginia Tech system with the following specifications, Precision 5820, 3700 MHz Xeon W-2145, 32 GB RAM, NVIDIA Quadro P400 is used.

The spanwise variation of sectional lift and drag coefficients is illustrated in following figures. Figure 4.5 and Figure 4.6 show the variation in normalized lift coefficient spanwise distribution at different angles of attack. The local drag distributions along the span, shown in Figure 4.7 and 4.8, show fluctuations at Mach number of 0.7, which can be due to modelling approximations and limitations of VSPAero at discretized cross sections. The variation at 0.8 Mach number is not fluctuating. This will need further investigations to address these unsatisfactory fluctuations, which can be studied considering sectional chordwise variations.

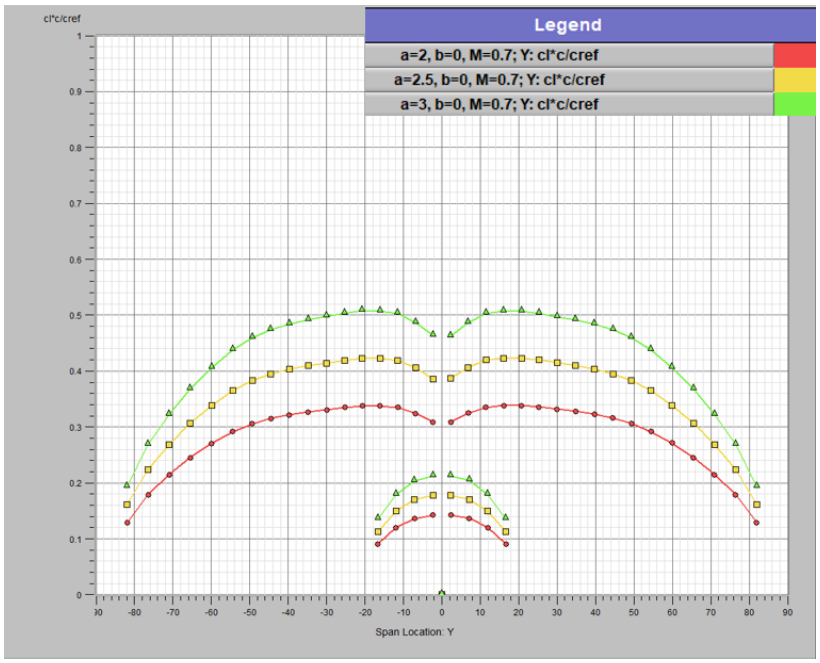

Figure 4.5: Variation of Normalised c_l distribution for α=2, 2.5 and 3 deg at M_∞=0.7 -CANW

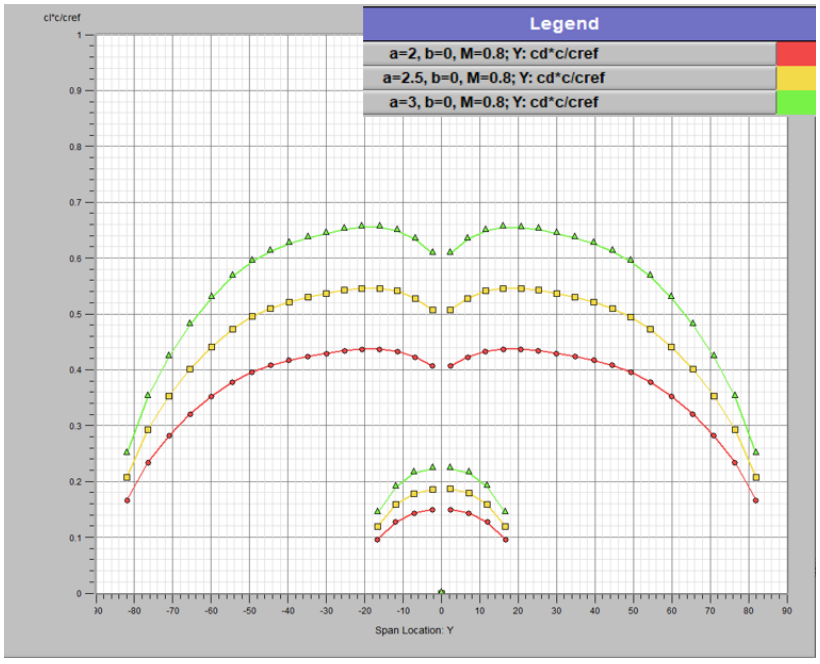

Figure 4.6: Variation of Normalised c_l distribution for α=2, 2.5 and 3 deg at M_∞=0.8 -CANW

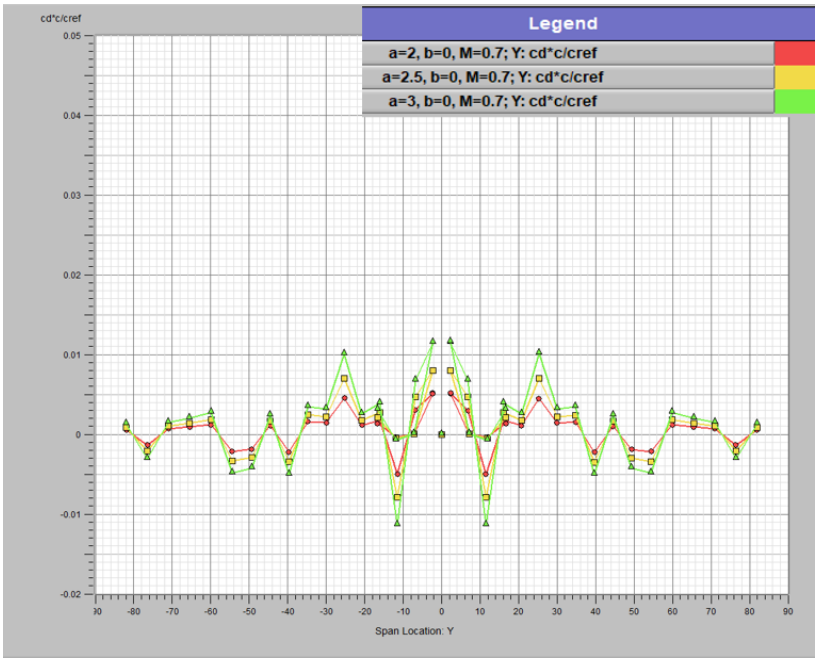

Figure 4.7: Variation of Normalised c_d distribution for α=2, 2.5 and 3 deg at M_∞=0.7 -CANW

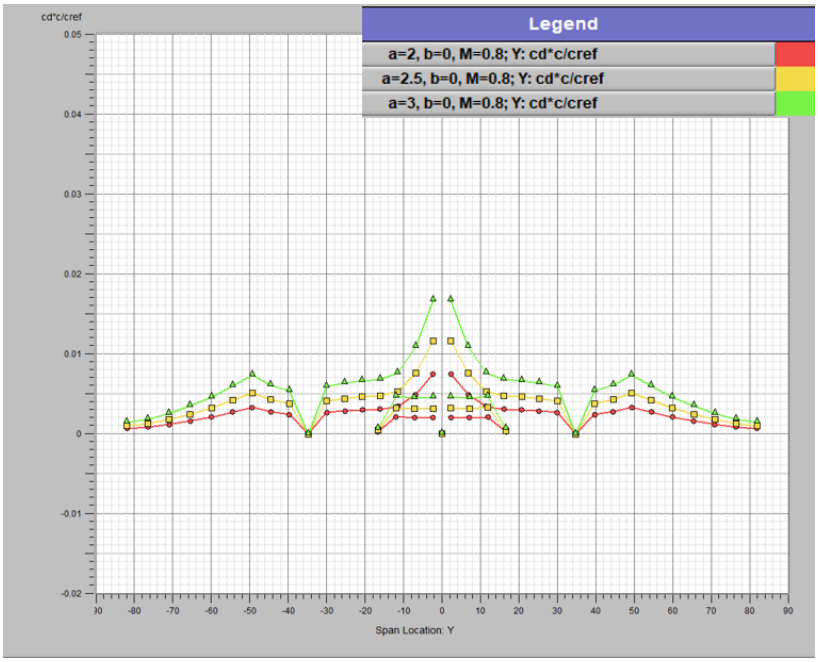

Figure 4.8: Variation of Normalised c_d distribution for α=2, 2.5 and 3 deg at M_∞=0.8 -CANW

4.2 Aerodynamic Results for SBW Configuration from VSPAero

This section discusses the results for the SBW configuration aircraft. The results are compared at different angle of attack and Mach number. The convergence for C_L, C_D and L/D is presented in Figure 4.9, 4.10 and 4.11, respectively. For the SBW configuration, the maximum C_L corresponds to the case of higher angle of attack at a given Mach number. VSPAero does not model flow separation beyond the critical angle of attack. A specialized method has been recently added which can help in stall modeling within VSP module. The maximum two-dimensional lift coefficient for a particular airfoil at a given flow, can be obtained from Theory of Wing Sections [27] and given as a constraint in the stall model tab. This will limit the local lift coefficients and model the non-linearity in lift curve at extreme angles of attack. The total drag coefficient value varies between 0.028 and 0.035. Similarly, The L/D

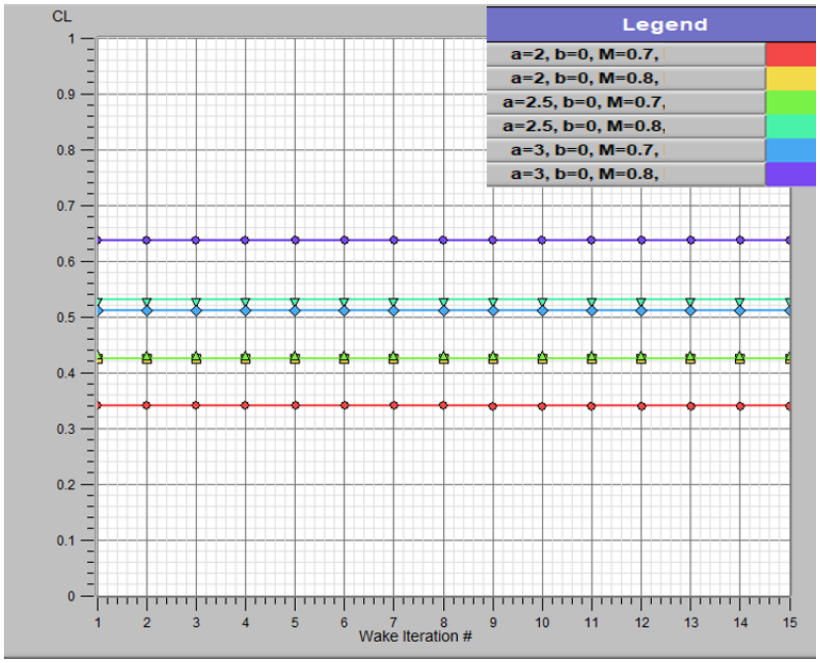

Figure 4.9: Convergence of C_L for α=2, 2.5 and 3 deg at M_∞=0.7 and 0.8 -SBW

ratio for SBW is between 12.25 and 18.25. The increase in L/D with an increase in the angle of attack is evident from Figure 4.11.

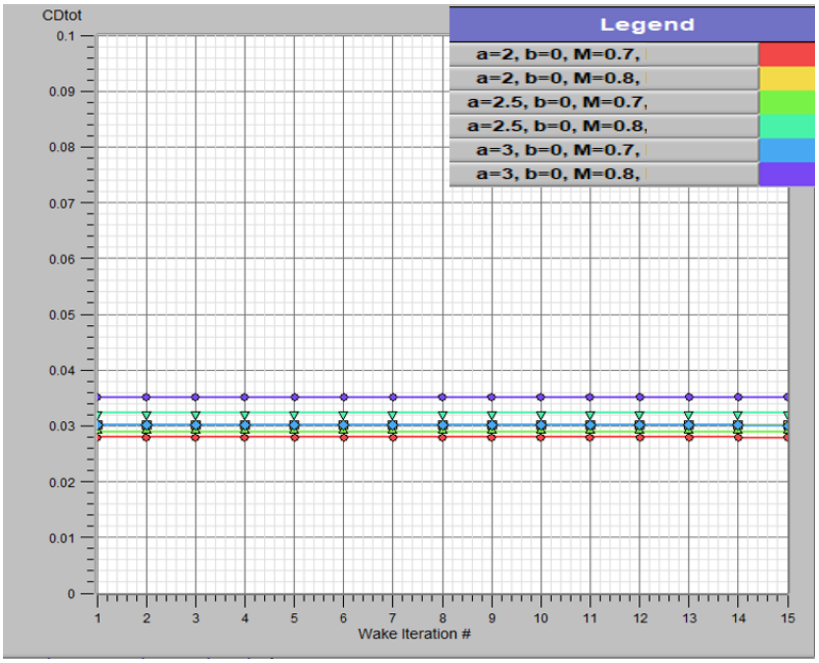

Figure 4.10: Convergence of C_D for α=2, 2.5 and 3 deg at M_∞=0.7 and 0.8 -SBW

It can be observed from the residual history for lift coefficient in Figure 4.12, that the convergence for the results can be considered appropriate. The residual is between 10^{-4} and 10^{-5}. The computation time taken for convergence is 7161.02 sec for the SBW configuration. This will be compared to other configurations with increase in complexity of the wing structure.

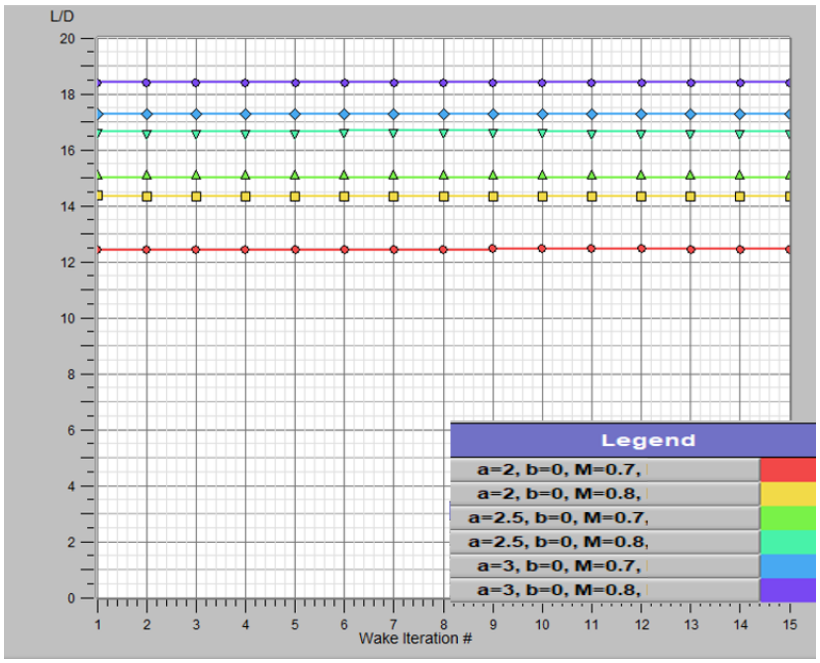

Figure 4.11: Convergence of L/D for α=2, 2.5 and 3 deg at M_∞=0.7 and 0.8 -SBW

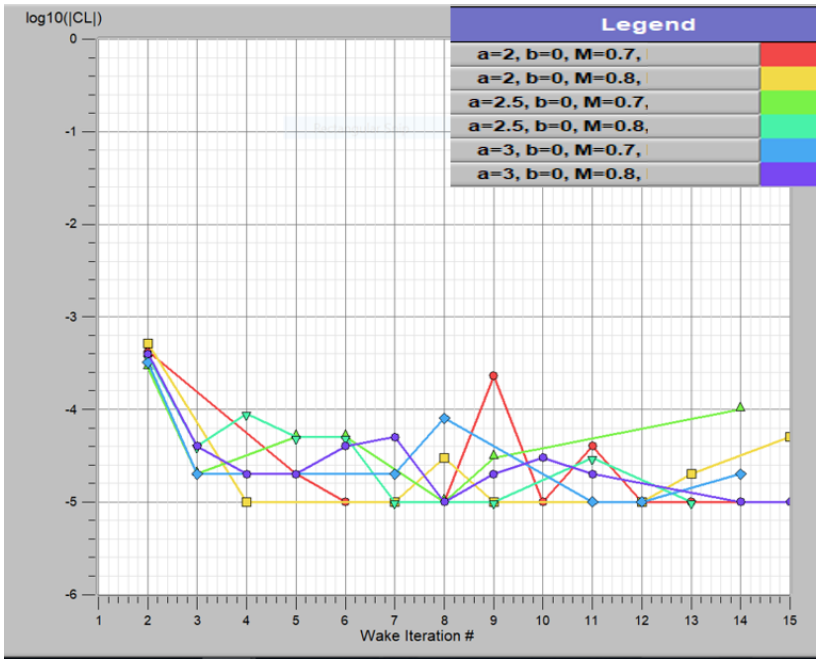

Figure 4.12: Residual for C_L for α=2, 2.5 and 3 deg at M_∞=0.7 and 0.8 -SBW

Figure 4.13 and 4.14 show the variation of normalised local lift coefficient along the span for the three angle of attack at M_∞=0.7 and 0.8. The distribution along the wing's span for M_∞=0.7 and 0.8 is consistent for varying angle of attack. The local lift coefficient increases as the Mach number and the angle of attack increase. The distribution along other lifting surfaces like the strut and the tail can be observed as well in the plots. The variation in main wing local drag coefficient is larger for the two different Mach number, when compared to the strut. The main wing accounts for approximately 80% of the lift generated.

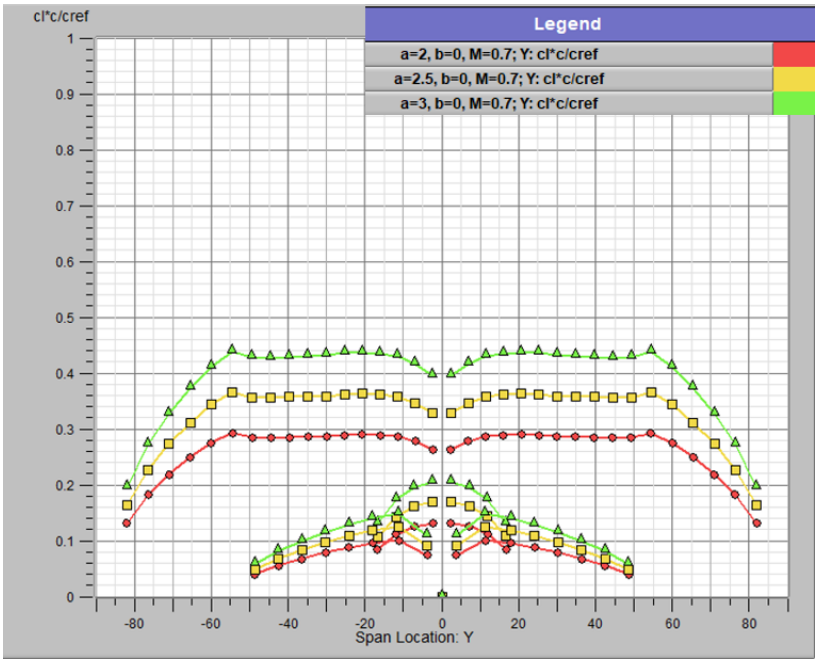

Figure 4.13: Variation of Normalised c_l distribution for α=2, 2.5 and 3 deg at M_∞=0.7 -SBW

Figure 4.15 and 4.16 show the variation of normalised local drag coefficient along the span for the three angle of attack at M_∞=0.7 and M_∞=0.8. The distribution is not smooth and fluctuating along the Y-axis of the wing for M_∞=0.7, whereas for M_∞=0.8, more consistent distribution can be observed. With an increase in the Mach number and angle of attack, an increase in local drag coefficient can be noticed.

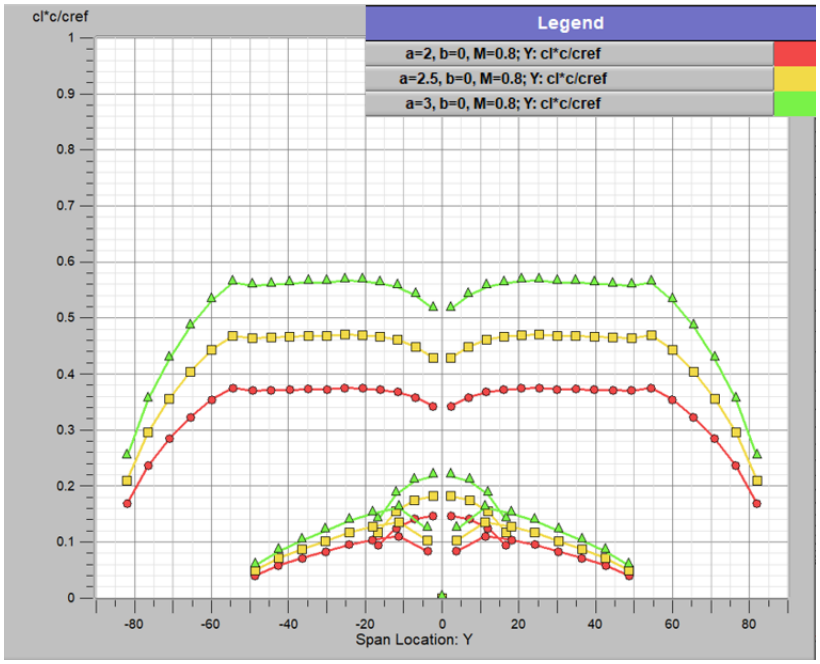

Figure 4.14: Variation of Normalised c_l distribution for α=2, 2.5 and 3 deg at M_∞=0.8 -SBW

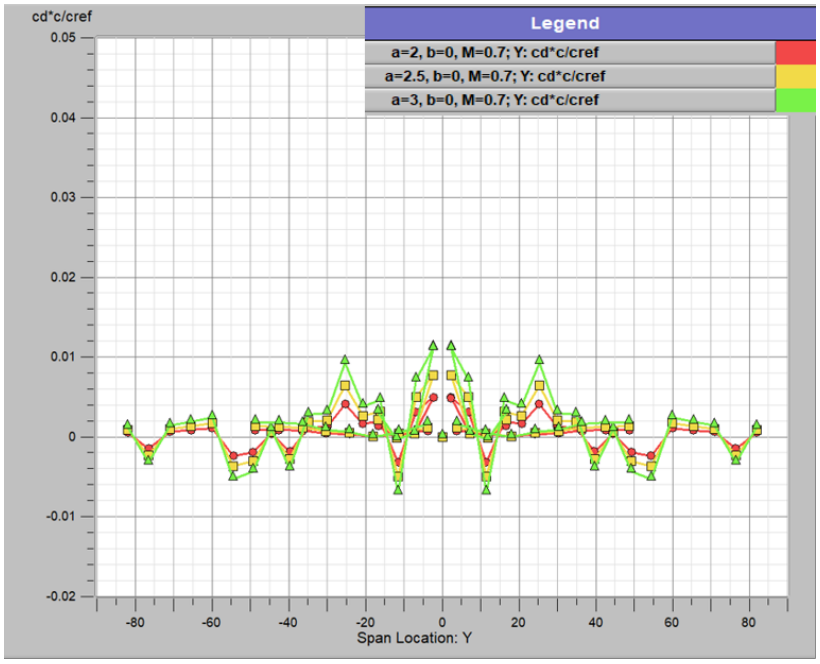

Figure 4.15: Variation of Normalised c_d distribution for α=2, 2.5 and 3 deg at M_∞=0.7 -SBW

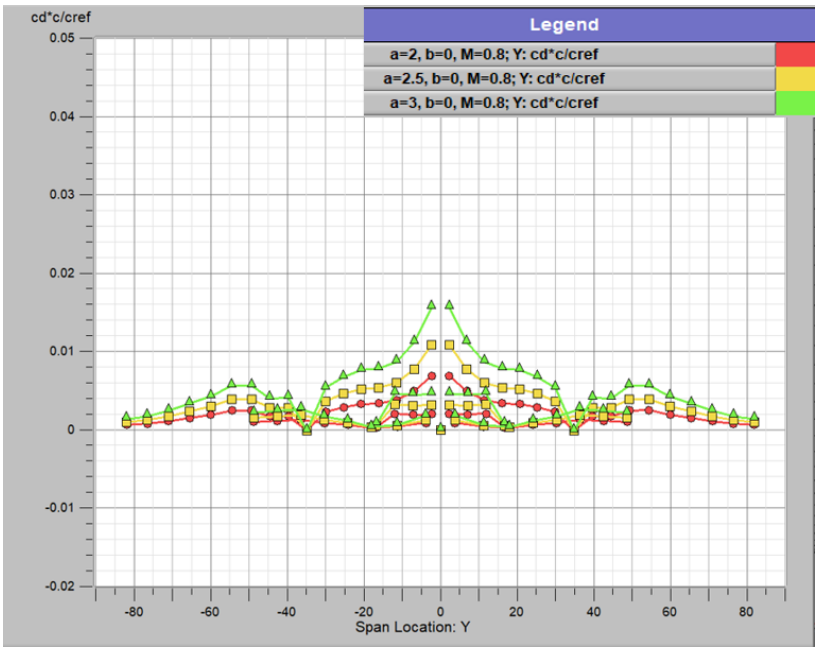

Figure 4.16: Variation of Normalised c_d distribution for α=2, 2.5 and 3 deg at M_∞=0.8 -SBW

Figure 4.17a to 4.19b illustrate the pressure coefficient variation Δc_p along the surfaces of the SBW aircraft configuration. The increase in Mach number shows a slightly higher negative pressure difference between top and bottom surface near the leading edge.

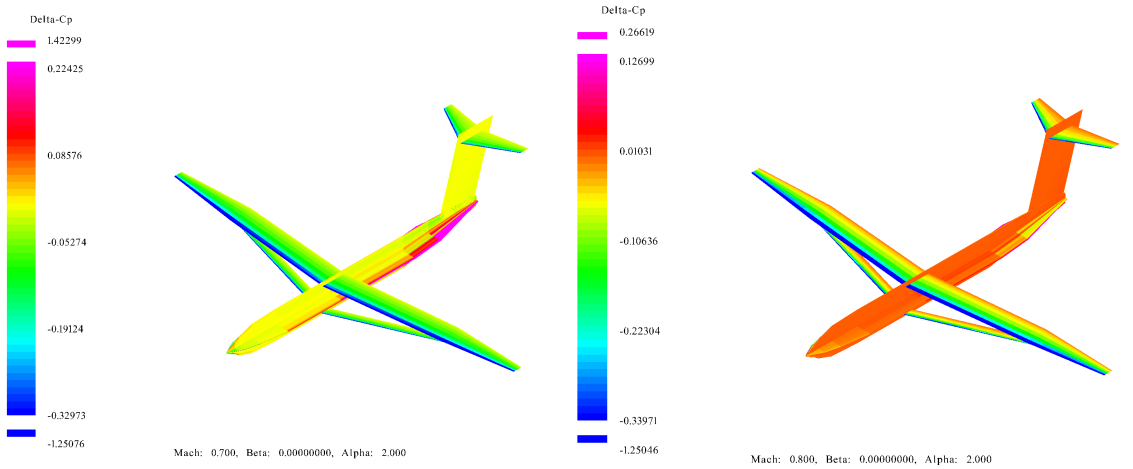

(a) (b)

Figure 4.17: Variation of Δc_p for α=2 deg at (a) M_∞=0.7 and (b) M_∞=0.8 -SBW

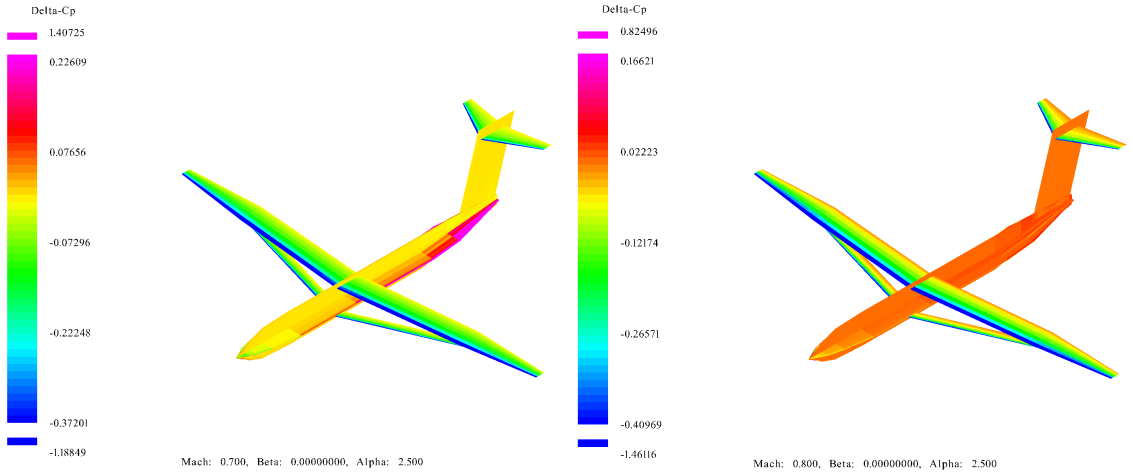

(a) (b)

Figure 4.18: Variation of Δc_p for α=2.5 deg at (a) M_∞=0.7 and (b) M_∞=0.8 -SBW

The variation with increase in Mach number can be seen for every angle of attack. The leading edge of strut displays suction regions, indicating possible lift generation.

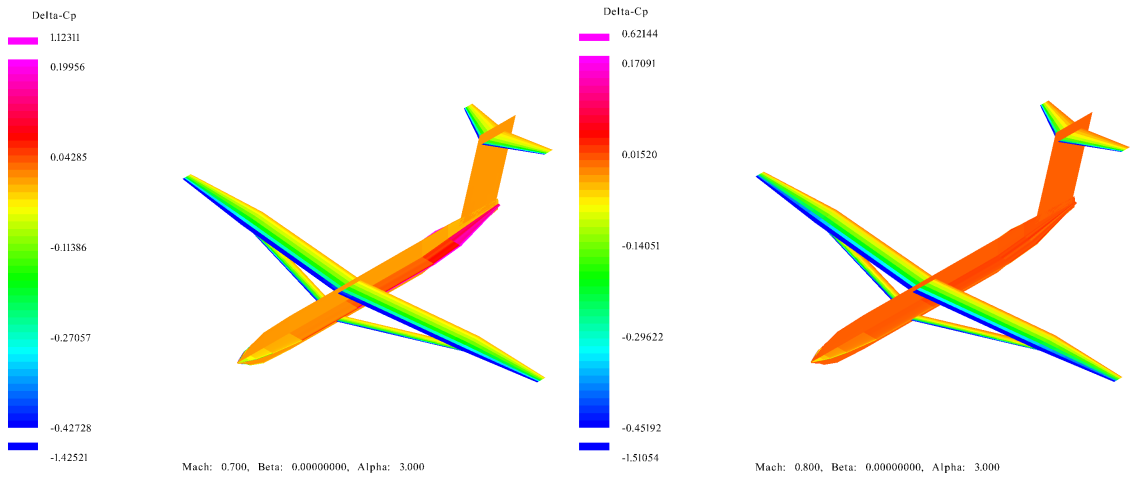

(a) (b)

Figure 4.19: Variation of Δc_p for α=3 deg at (a) M_∞=0.7 and (b) M_∞=0.8 -SBW

4.3 Aerodynamic Results for TBW Configuration from VSPAero

4.3.1 Aerodynamic Results for TBW-I Configuration

This section discusses the results for the TBW-I configuration aircraft. The results are computed and compared at different values of angle of attack and Mach number. The convergence for C_L, C_D and L/D is presented in Figure 4.20, 4.21 and 4.22, respectively. The case of α=2.5 deg at M_∞=0.8 has a higher lift coefficient compared to that of the case of α=3 deg at M_∞=0.7. However, it can be interpreted from Figure 4.21 that drag is significantly lower for the latter case. As a result, we can see that for the lift-over-drag ratio, the trend is reversed. The L/D for the former case is lower.

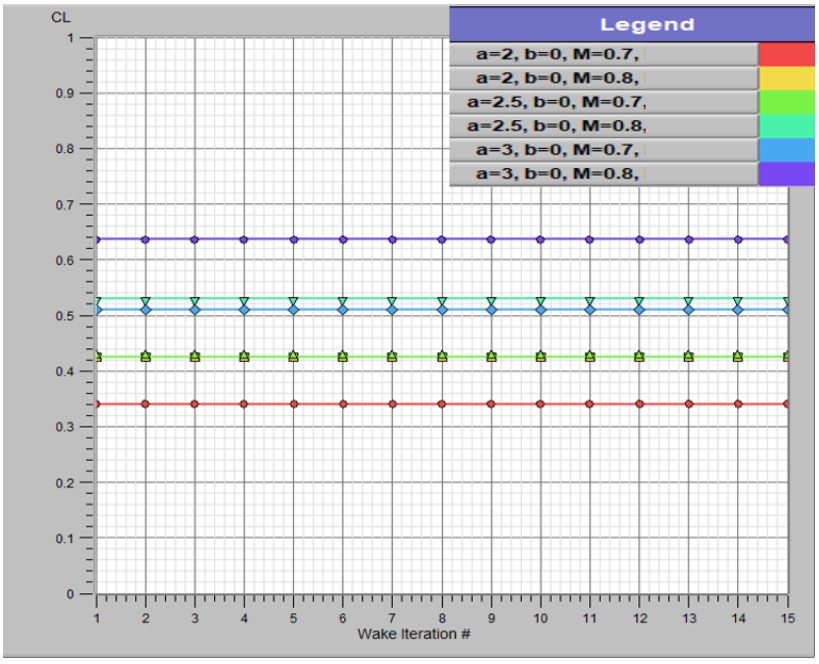

Figure 4.20: Convergence of C_L for α=2, 2.5 and 3 deg at M_∞=0.7 and 0.8 -TBW-I

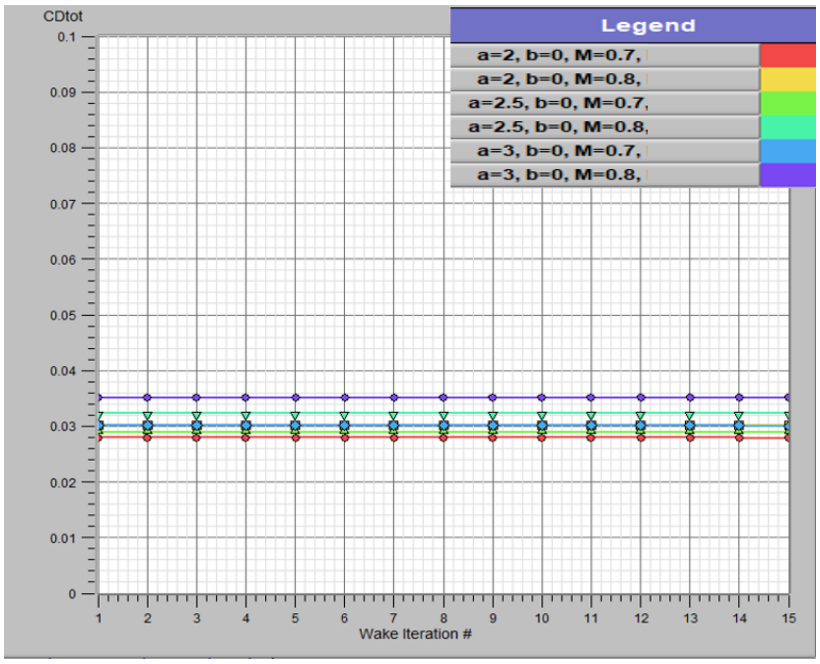

Figure 4.21: Convergence of C_D for α=2, 2.5 and 3 deg at M_∞=0.7 and 0.8 -TBW-I

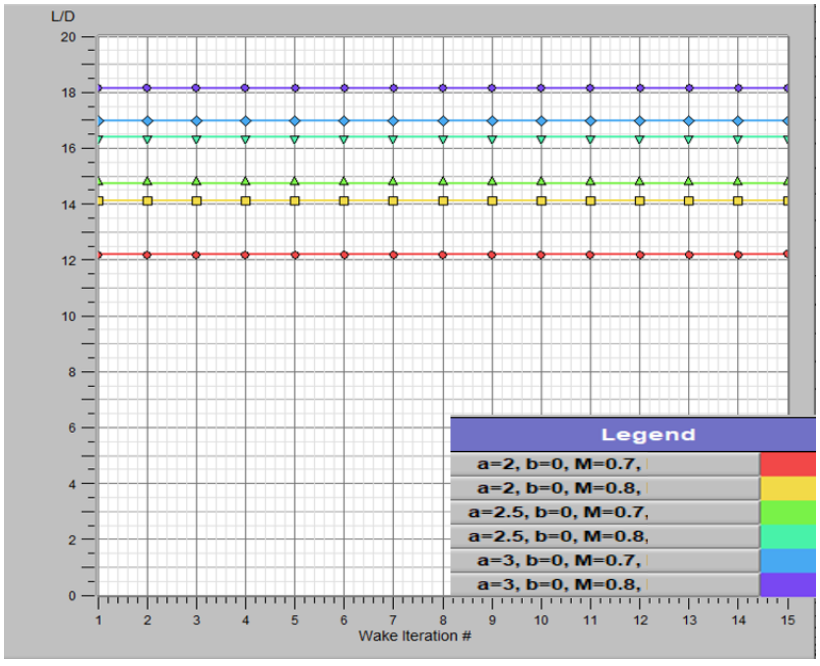

Figure 4.22: Convergence of L/D for α=2, 2.5 and 3 deg at M_∞=0.7 and 0.8 -TBW-I

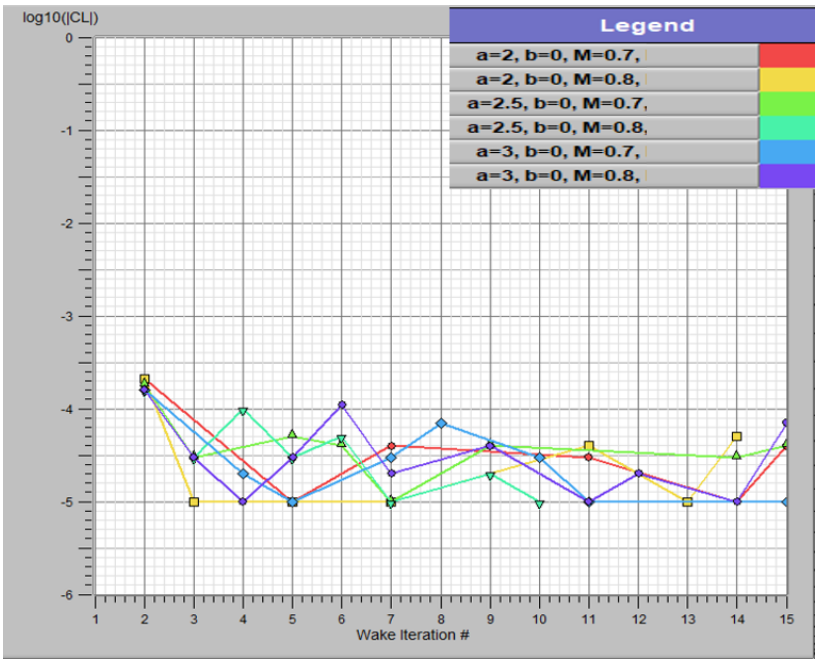

Figure 4.23: Residual for C_L for α=2, 2.5 and 3 deg at M_∞=0.7 and 0.8 -TBW-I

For the TBW-I configuration, the variation of normalised local lift coefficient along the span for the three angle of attack at M_∞=0.7 and M_∞=0.8 is presented in Figure 4.24 and 4.25. Similar to the case of SBW configuration, the trend of consistent distribution along Y-axis of the wing at M_∞=0.7 and M_∞=0.7 for varying angle of attack, is observed here. The local lift coefficient increases as the Mach number and angle of attack increase. Approximately, 24% increase can be noticed in the maximum local lift coefficient for same angle of attack as the flow Mach number increases from 0.7 to 0.8. The spanwise distribution for the strut, the additional jury and the tail is demonstrated in these figures. The variation in the main wing local lift coefficient is larger for the two different Mach numbers, when compared to its value for strut and the jury. The contribution of the jury member to the lift is negligible.

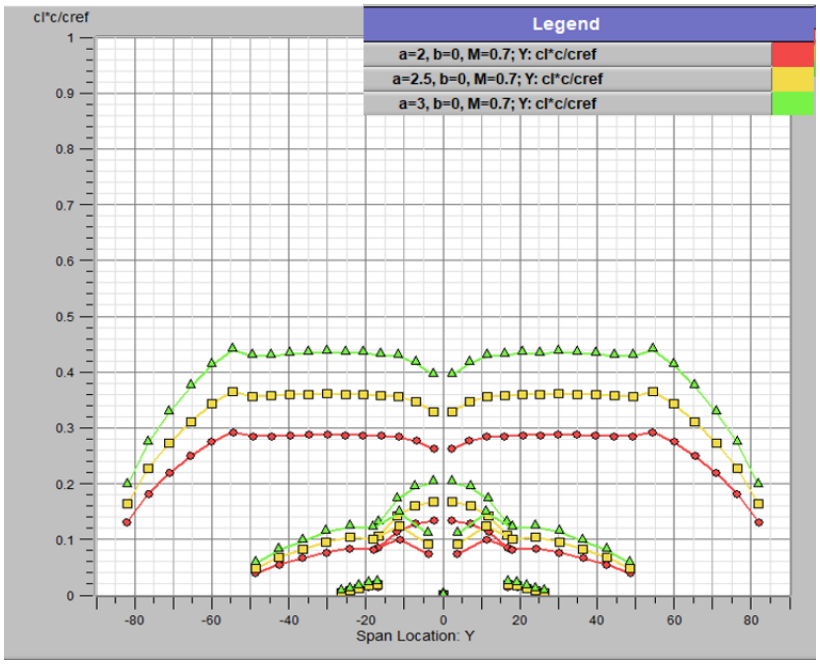

Figure 4.24: Variation of Normalised c_l distribution for α=2, 2.5 and 3 deg at M_∞=0.7 -TBW-I

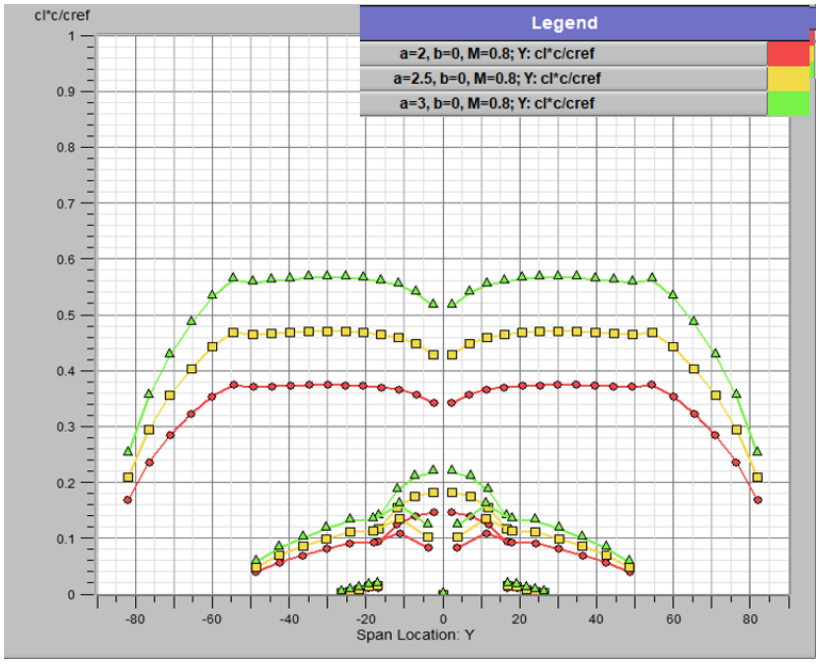

Figure 4.25: Variation of Normalised c_l distribution for α=2, 2.5 and 3 deg at M_∞=0.8 -TBW-I

The addition of jury further disrupts the local drag coefficient distribution as shown in Figure 4.26. There is not much increase in the maximum local drag efficient between the cases of the two Mach numbers. Figure 4.27 shows the normalised local drag coefficient distribution for varying angle of attack at M_∞=0.8.

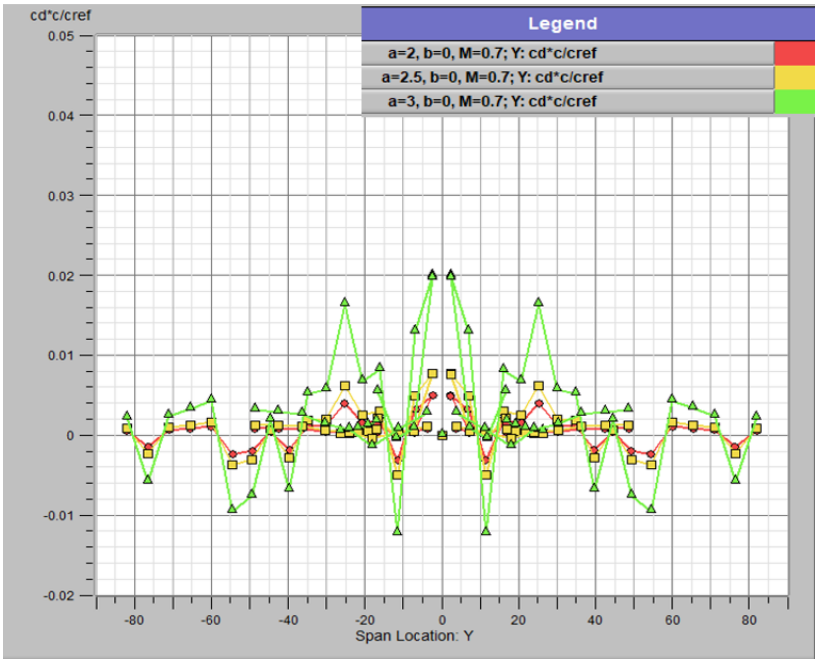

Figure 4.26: Variation of Normalised c_d distribution for α=2, 2.5 and 3 deg at M_∞=0.7 -TBW-I

Figure 4.28a to 4.30b show the pressure coefficient, Δc_p, variation along the surfaces of the aircraft for the TBW-I configuration. The evidence can be illustrated that the strut and jury have decent negative Δc_p near the leading edge. This suggests that the supporting members generate a significant amount of lift, which must be accounted for.

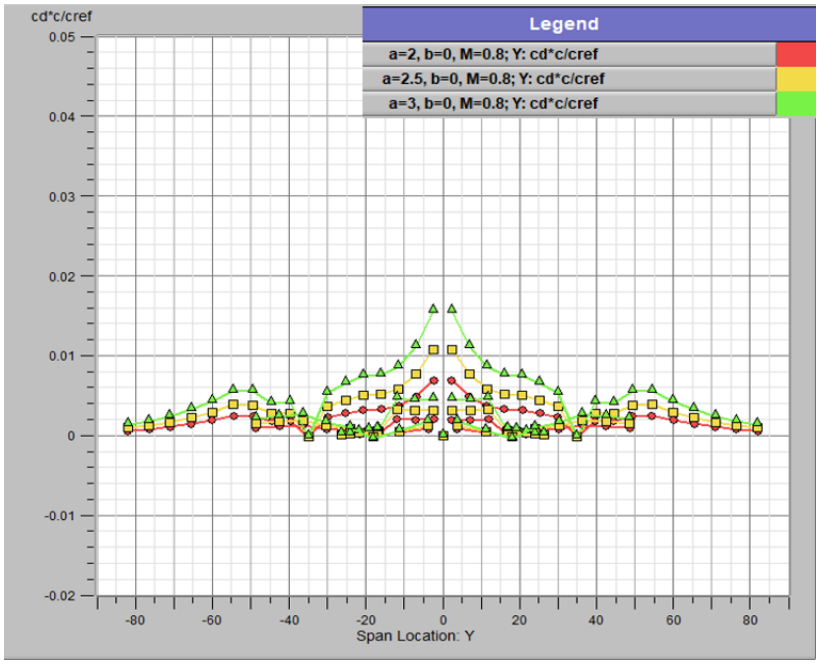

Figure 4.27: Variation of Normalised c_d distribution for α=2, 2.5 and 3 deg at M_∞=0.8 -TBW-I

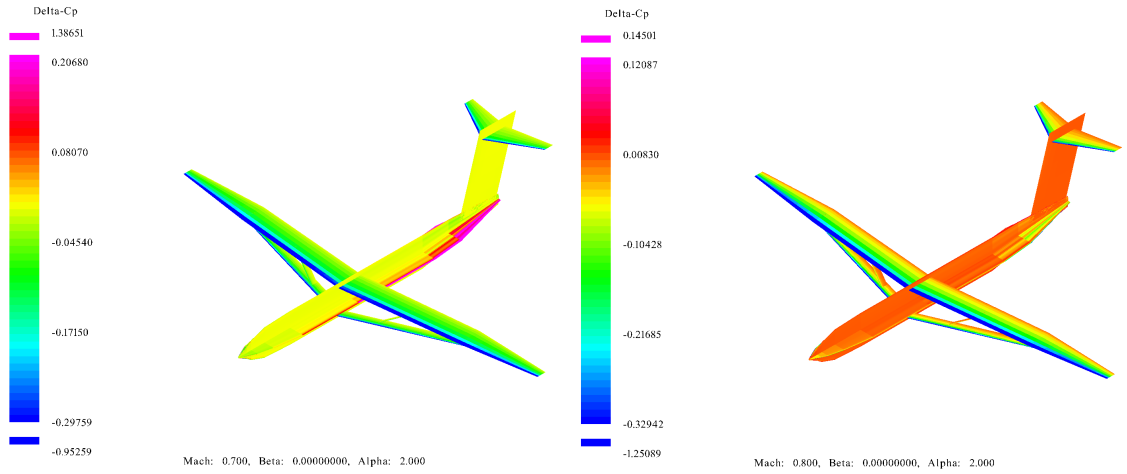

(a) (b)

Figure 4.28: Variation of Δc_p for α=2 deg at (a) M_∞=0.7 and (b) M_∞=0.8 -TBW-I

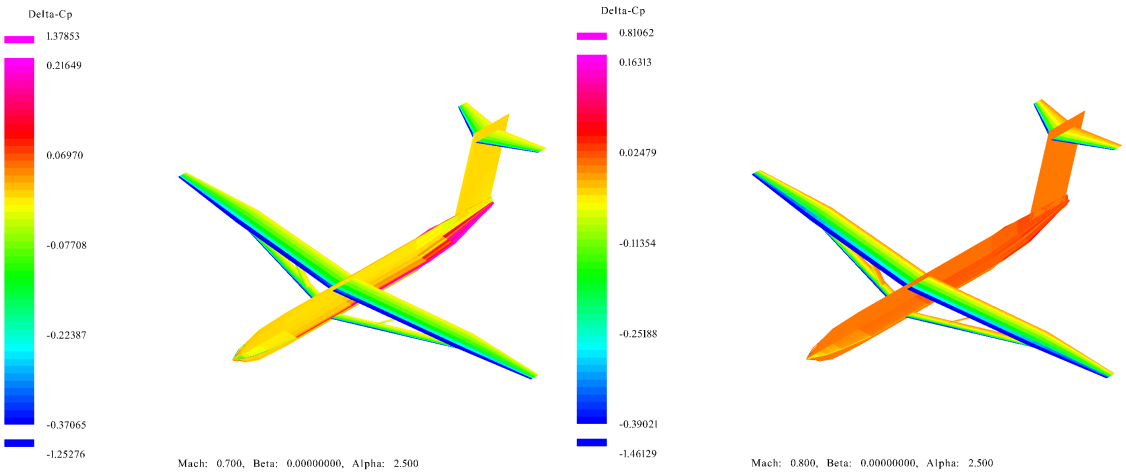

(a) (b)

Figure 4.29: Variation of Δc_p for α=2.5 deg at (a) M_∞=0.7 and (b) M_∞=0.8 -TBW-I

The previous studies assumed no lift on the strut and jury. Hence, the need to consider strut and jury as lifting surfaces can be justified. The strut has a better gradient than compared to the jury.

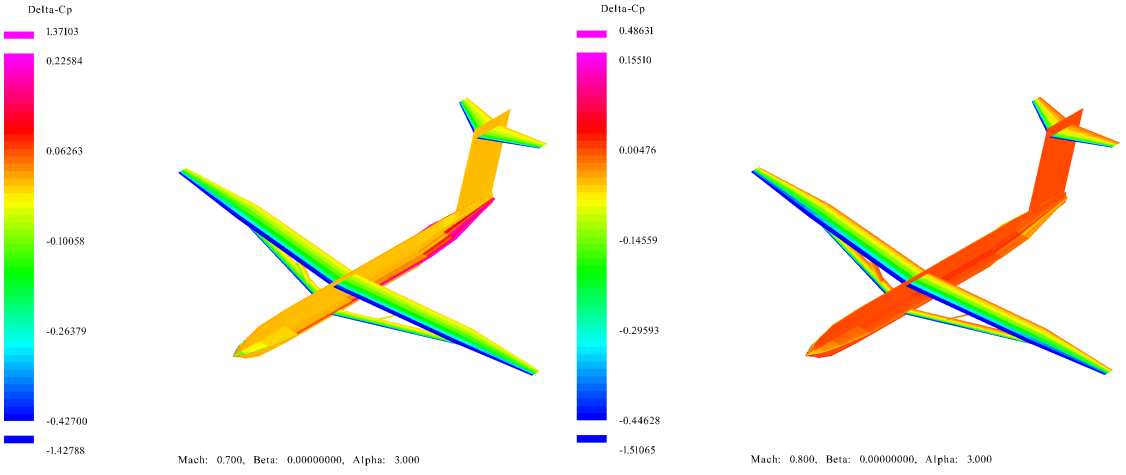

(a) (b)

Figure 4.30: Variation of Δc_p for α=3 deg at (a) M_∞=0.7 and (b) M_∞=0.8 -TBW-I

4.3.2 Aerodynamic Results for TBW-II Configuration

This section discusses the results for TBW-II configuration with a larger wing span. A trend similar for TBW-I configuration, is observed for the lift coefficient values of TBW-II for varying angle of attack and Mach number. Figure 4.31 shows that the corresponding lift coefficient values are higher for this configuration.

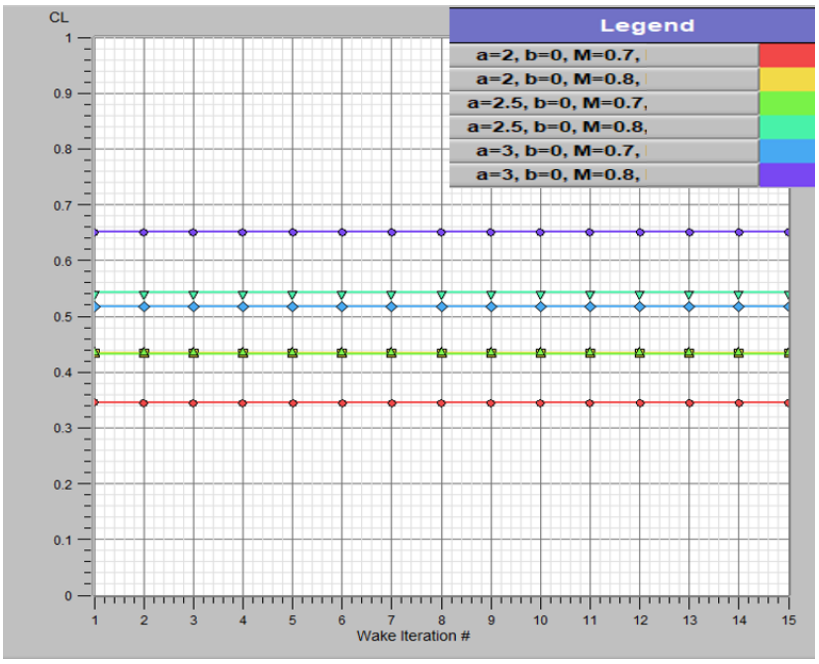

Figure 4.31: Convergence of C_L for α=2, 2.5 and 3 deg at M_∞=0.7 and 0.8 -TBW-II

However, as a result of increased aspect ratio, the difference in drag for the two cases is reversed. This results in a higher L/D ratio for the case of α =2.5 deg at M_∞=0.8 than that compared to the case of α =3 deg at M_∞=0.7, as shown in Figure 4.33. This is opposite to what was observed in the case of the TBW-I configuration.

Figure 4.34 shows the residual history for the convergence of lift coefficient. The residual values are slightly lower compared to the previous two cases, suggesting that the convergence

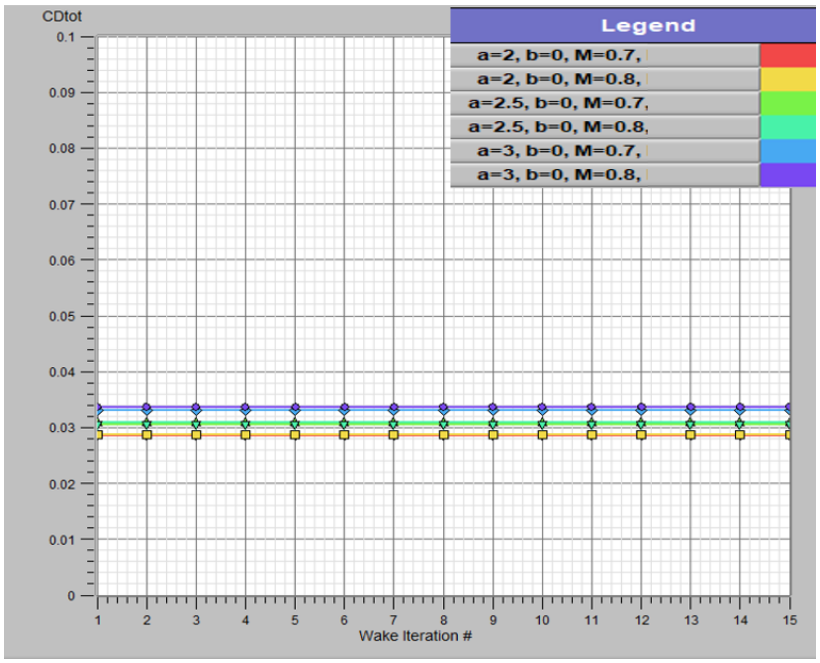

Figure 4.32: Convergence of C_D for α=2, 2.5 and 3 deg at M_∞=0.7 and 0.8 -TBW-II

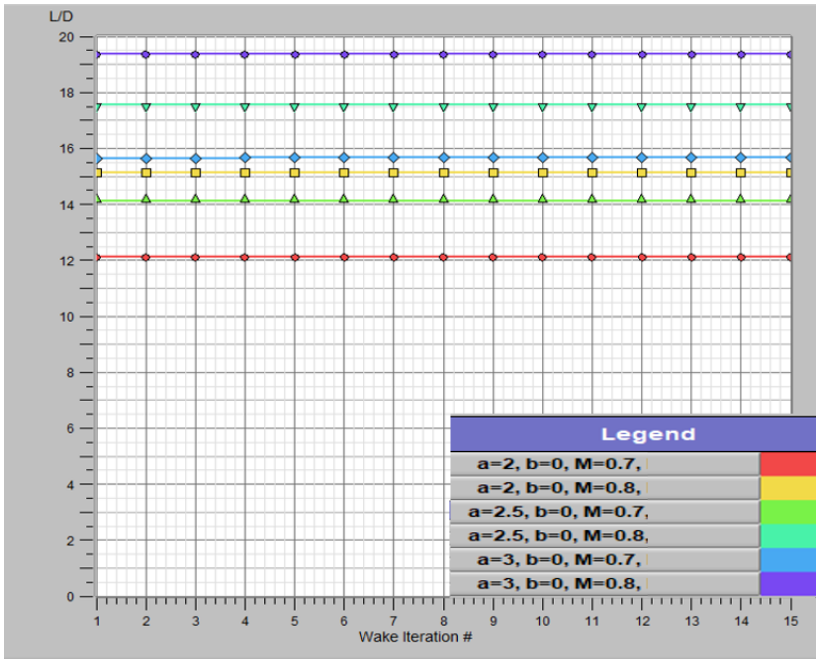

Figure 4.33: Convergence of L/D for α=2, 2.5 and 3 deg at M_∞=0.7 and 0.8 -TBW-II

was better. The time taken for convergence was around 12341.5 sec, which is 72.34% higher than that taken by SBW configuration calculations.

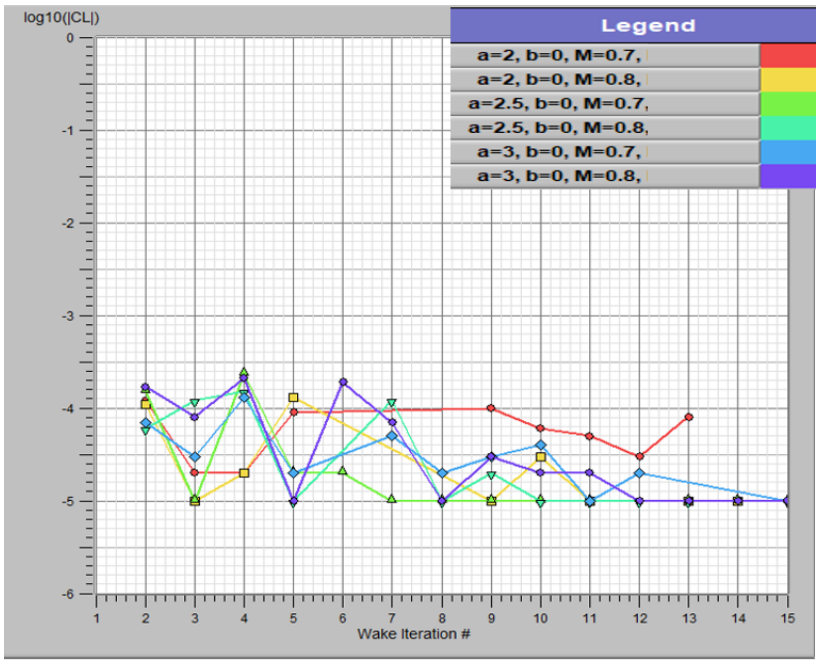

Figure 4.34: Residual for C_L for α=2, 2.5 and 3 deg at M_∞=0.7 and 0.8 -TBW-II

The local lift coefficient goes up slightly with the increased span for the new configuration. The variation and maximum for c_l is demonstrated in Figure 4.35 and 4.36. There is no significant change in the contribution from the strut and the jury, despite the increase in span for the member wings as well.

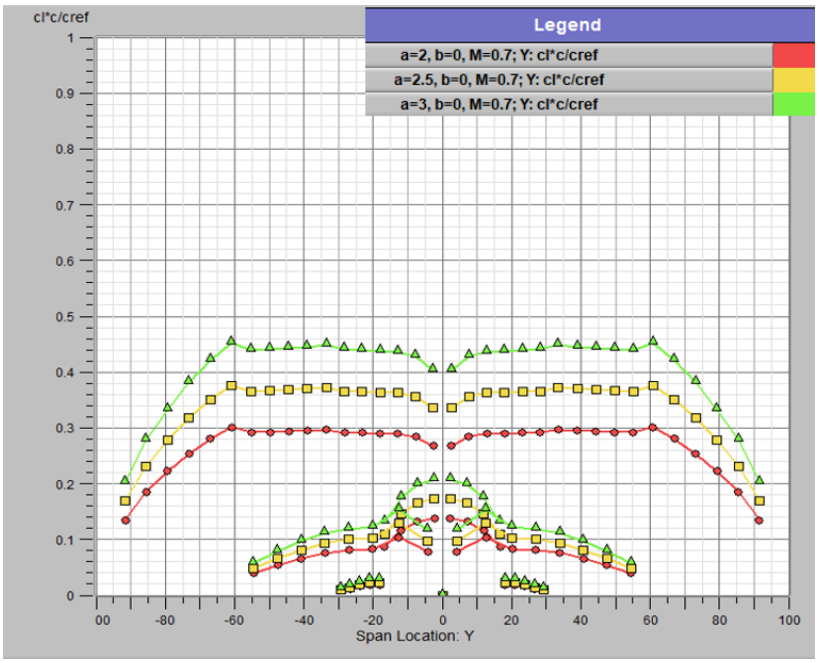

Figure 4.35: Variation of Normalised c_l distribution for α=2,2.5 and 3 deg at M_∞=0.7 - TBW-II

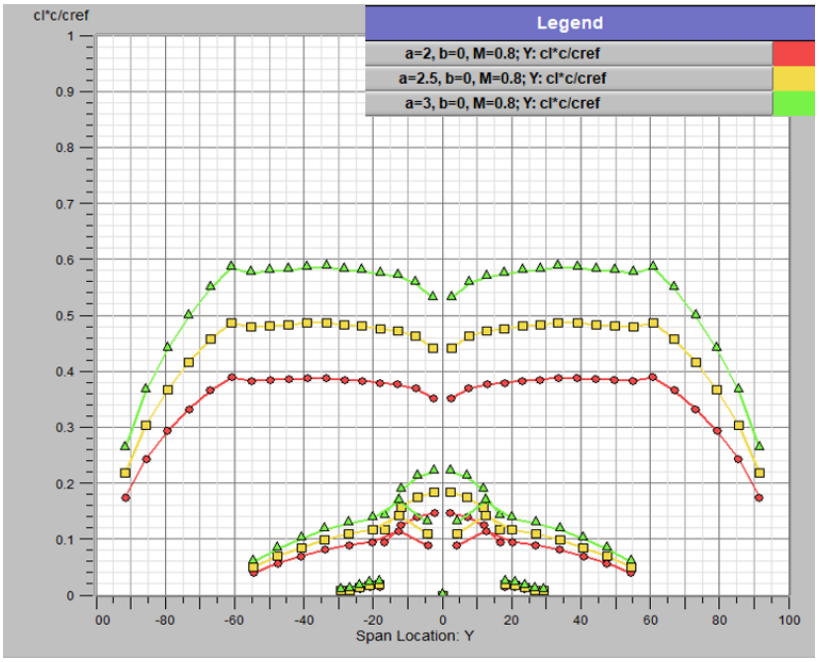

Figure 4.36: Variation of Normalised c_l distribution for α=2,2.5 and 3 deg at M_∞=0.8 - TBW-II

Figure 4.37 shows the normalised local drag coefficient distribution for varying angle of attack at M_∞=0.7 for TBW-II configuration. Compared to TBW-I, no negative local drag coefficient can be observed here. The distribution is still not consistent along the Y-axis. A small increase in local drag coefficient at the wing tip is observed in Figure 4.38. This may be attributed to the high vorticity near the tip.

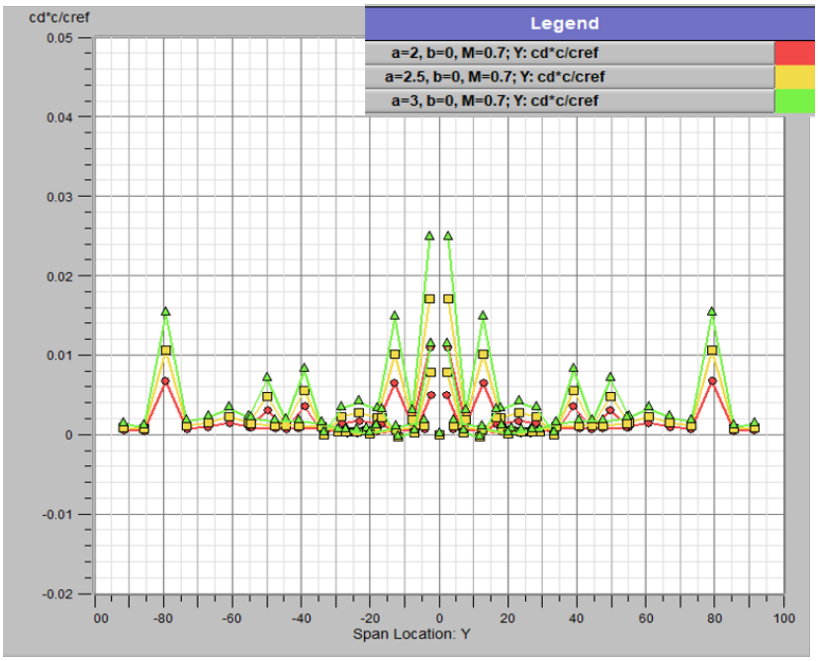

Figure 4.37: Variation of Normalised c_d distribution for α=2, 2.5 and 3 deg at M_∞=0.7 -TBW-II

Figure 4.39a to Figure 4.41b show the variation in Δc_p for TBW-II configuration. The addition of jury, coupled with the increase in strut span, decreases the Δc_p for all angle of attack when compared to previous configurations in this study.

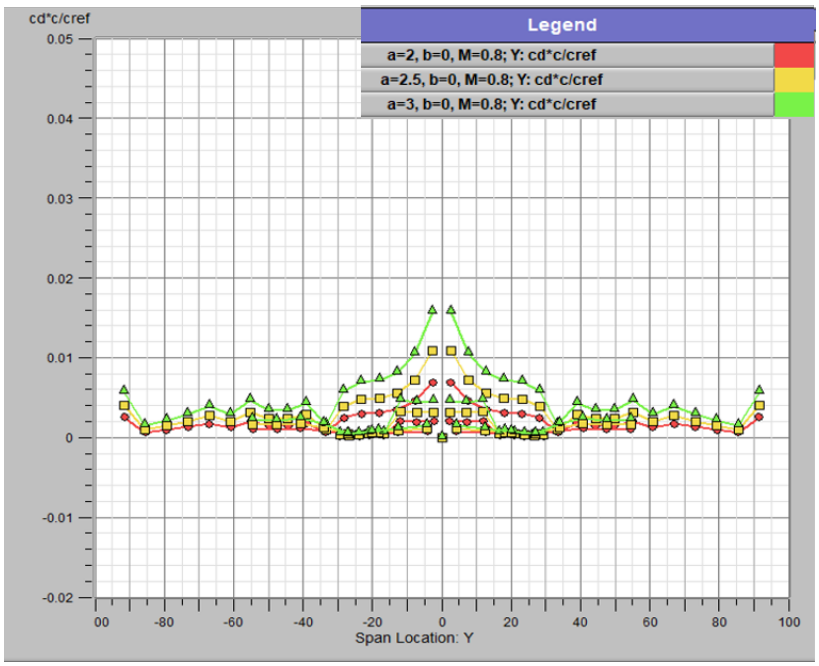

Figure 4.38: Variation of Normalised c_d distribution for α=2, 2.5 and 3 deg at M_∞=0.8 -TBW-II

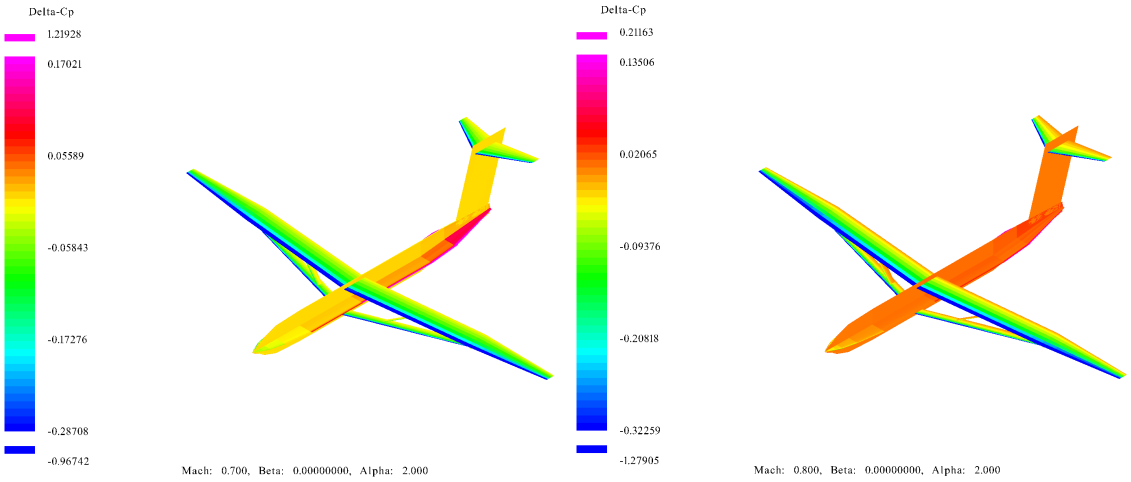

(a) (b)

Figure 4.39: Variation of Δc_p for α=2 deg at (a) M_∞=0.7 and (b) M_∞=0.8 -TBW-II

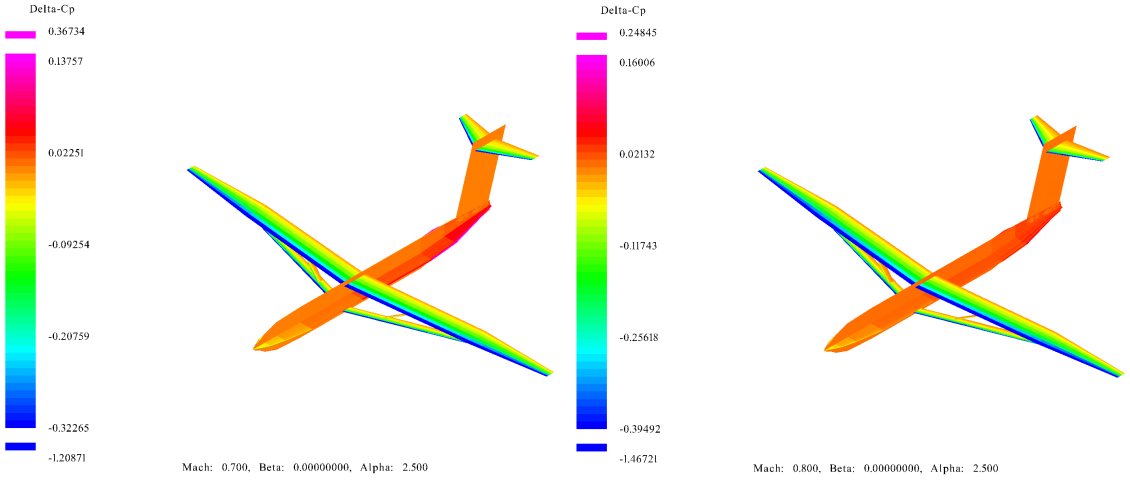

(a) (b)

Figure 4.40: Variation of Δc_p for α=2.5 deg at (a) M_∞=0.7 and (b) M_∞=0.8 -TBW-II

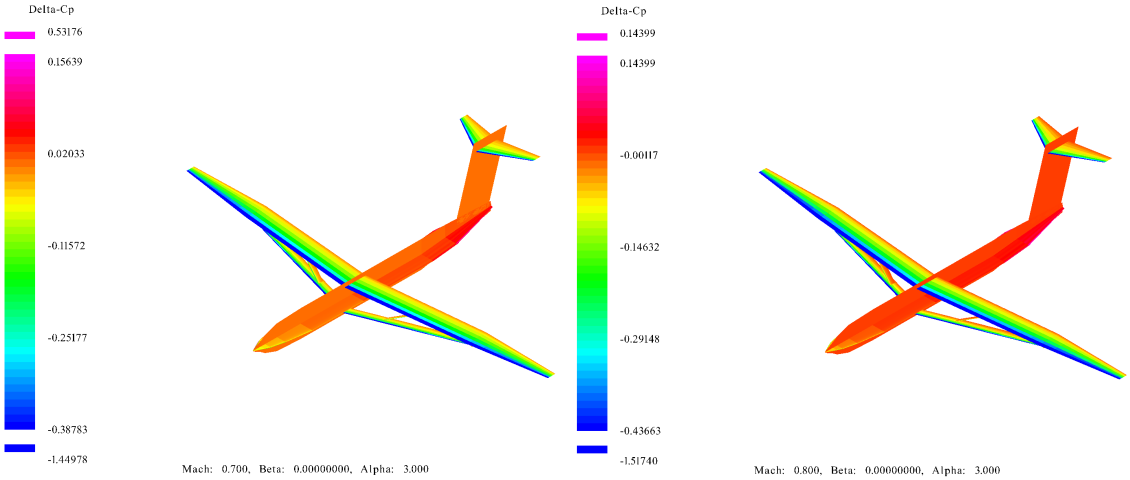

(a) (b)

Figure 4.41: Variation of Δc_p for α=3 deg at (a) M_∞=0.7 and (b) M_∞=0.8 -TBW-II

4.4 Coefficients and Stability Derivatives

A Flight Dynamics model needs aerodynamic coefficients and stability derivatives. VSPAero is used to estimate these coefficients and derivatives. Some of the coefficients and derivatives have been tabulated in this section. Table 4.1 to Table 4.6 display the coefficients for varying Mach number and corresponding angle of attack for different configurations. Not much difference is observed between SBW and TBW configurations. TBW-II configurations shows increase in lift and drag coefficients.

Table 4.1: Coefficients for SBW aircraft configuration at M_∞=0.7

	M_∞=0.7		
Coefficients	α=2 deg	α=2.5 deg	α=3 deg
C_L	0.3399	0.4254	0.5105
C_D	0.0012	0.0020	0.0029
C_S	-0.0009	-0.0007	-0.00002
$C_{L_{roll}}$	-0.0123	-0.0021	-0.0001
C_M	-78.297	-10.473	-0.9641
C_N	0.3055	0.0503	0.0016

Table 4.2: Coefficients for SBW aircraft configuration at M_∞=0.8

	M_∞=0.8		
Coefficients	α=2 deg	α=2.5 deg	α=3 deg
C_L	0.4248	0.5309	0.6369
C_D	0.0032	0.0051	0.0073
C_S	0.0003	0.00004	-0.00003
$C_{L_{roll}}$	-0.0004	0.00003	-0.00003
C_M	-0.2760	0.2533	0.2973
C_N	0.0179	-0.0011	0.0008

Table 4.3: Coefficients for TBW aircraft configuration at M_∞=0.7

	M_∞=0.7		
Coefficients	α=2 deg	α=2.5 deg	α=3 deg
C_L	0.3401	0.4252	0.5103
C_D	0.0013	0.0020	0.0029
C_S	-0.0002	-0.0010	-0.0005
$C_{L_{roll}}$	-0.0021	-0.0025	-0.0003
C_M	-14.588	-9.2588	-2.8976
C_N	0.0514	0.0615	0.0063

Table 4.4: Coefficients for TBW aircraft configuration at M_∞=0.8

	M_∞=0.8		
Coefficients	α=2 deg	α=2.5 deg	α=3 deg
C_L	0.4245	0.5305	0.6366
C_D	0.0032	0.0051	0.0073
C_S	0.00006	0.0002	0.00006
$C_{L_{roll}}$	0.00007	0.0003	0.00003
C_M	0.2309	0.2304	0.2820
C_N	-0.0045	-0.0013	0.0002

Table 4.5: Coefficients for TBW-II aircraft configuration at M_∞=0.7

	M_∞=0.7		
Coefficients	α=2 deg	α=2.5 deg	α=3 deg
C_L	0.3451	0.4315	0.5178
C_D	0.0032	0.0050	0.0072
C_S	-0.0001	-0.0003	-0.0003
$C_{L_{roll}}$	0.00003	-0.00002	0.00006
C_M	-0.7164	0.1759	0.2203
C_N	-0.0022	0.0002	-0.0019

Table 4.6: Coefficients for TBW-II aircraft configuration at M_∞=0.8

	M_∞=0.8		
Coefficients	α=2 deg	α=2.5 deg	α=3 deg
C_L	0.4339	0.5425	0.6508
C_D	0.0031	0.0049	0.0071
C_S	-0.00003	0.00005	-0.00003
$C_{L_{roll}}$	-0.000005	0.000002	-0.000005
C_M	0.1612	0.0883	0.1171
C_N	0.0001	-0.00004	0.0001

Table 4.7 and 4.8 illustrate the stability derivatives obtained for different configurations for a steady analysis. These tables present the lift and drag derivatives for the SBW, TBW-I and TBW-II at α= 2.5 deg. The SBW and TBW-I configurations do not indicate a significant difference for these derivatives. However, TBW-II shows significant increase in Angle-of-Attack lift effectiveness and Angle-of-Attack drag effectiveness compared to previous configurations.

Table 4.7: C_L Derivatives for different aircraft configurations

	Configurations		
Derivatives	SBW	TBW-I	TBW-II
C_{L_α}	9.7157	9.7420	9.8645
C_{L_β}	-0.0169	-0.0071	-0.0273
C_{L_p}	0.0229	0.0331	0.0193
C_{L_q}	4.7126	4.2662	4.1416
C_{L_r}	0.0472	0.0516	0.0457
$C_{L_{M_\infty}}$	1.0553	1.0536	1.1102
C_{L_u}	0.7387	0.7375	0.7771

Unit for all derivatives is per rad, except for M_∞ and u

Table 4.8: C_D Derivatives for different aircraft configurations

	Configurations		
Derivatives	SBW	TBW-I	TBW-II
C_{D_α}	0.1101	0.1108	0.2745
C_{D_β}	0.0223	0.0340	-2.19041
C_{D_p}	-0.1704	-0.2910	-0.1571
C_{D_q}	-0.4290	-1.0638	-0.5734
C_{D_r}	-0.0298	0.0417	-0.0217
$C_{D_{M_\infty}}$	0.0305	0.0304	-0.0009
C_{D_u}	0.0213	0.0213	-0.0007

Unit for all derivatives is per rad, except for M_∞ and u

A detailed output for coefficients and stability derivatives obtained from VSPAero is given in Appendix B.

4.5 Discussion

The derivative C_{L_α} for these results is compared to the ones obtained using the superposition approach and the CFD studies using USM3D and FUN3D [3]. Table 4.9 shows the variation in values obtained from different methods. The base angle of attack for this particular

Table 4.9: TBW lift curve slope comparison

	C_{L_α}	C_{L_α} % Difference
FUN3D	9.8225	1.59
USM3D (lim off)	9.9807	0
USM3D (lim on)	9.6230	3.58
VORLAX (Full Configuration)	6.0526	39.36
VORLAX (Superposition 1)	9.4097	5.72
VORLAX (Superposition 1)	9.3707	6.11
OpenVSP (TBW-I)	9.7420	2.39

comparison is 2.5 deg for TBW-I configuration. This is keeping in mind the configuration used in the comparison study. It is evident from the above results that there is an excellent agreement for C_{L_α} with the CFD results. The % difference is less than approximately 2.5%. However, the results do not show a good agreement for the lift coefficient itself. This may be due to modeling differences and approximations in parameters.

The OpenVSP tool has certain limitations with respect to the flow conditions and the input parameters. The VSPAero module implements either VLM or Panel method. The limitation for applications with respect to Mach number is M_∞=0 to 5, as limits for the tool.

As the VSPAero module is based on linear potential flows, it lacks the capability to model transonic and viscous effects. Since the aircraft speed considered here is between Mach=0.7 and 0.8, it is necessary to account for wave and viscous drag and transonic effects on lift and induced drag. Transonic small disturbances can be considered to account for these transonic effects. The surface pressure and the velocity are calculated for upper and lower airfoil by

incorporating transonically-scaled potential. TSFOIL [28], an open-source transonic flow model has been implemented in a study [5]. The updated pressure coefficient is integrated to compute the aerodynamic coefficient for lift and induced drag. The TSD is implemented at each section for the effective 2D angle of attack.

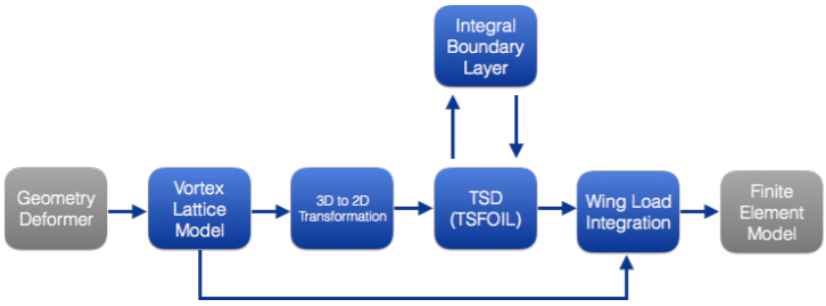

Figure 4.42: Integrated Aerodynamics model for transonic application [5]

Figure 4.42 shows the model framework to account for transonic effects and viscous effects after the VLM model is implemented. The updated pressure coefficient from TSD model is fed to Integral Boundary Layer model which computes the boundary layer displacement thickness. This added thickness is updated to obtain the pressure coefficient distribution. The new thickness is calculated based on this updated pressure coefficient distribution. This process iterates until convergence for thickness and pressure coefficient distribution is achieved. The steps are repeated until the VLM sectional lift and airfoil lift from the integrated TSD/IBL model converges for all sections. This new set of aerodynamic parameters can be used for further integration with structural model for flight dynamic analysis.

The derivatives and coefficient values for different configurations shown here, demonstrate that OpenVSP can serve as a useful tool for preliminary and computationally inexpensive aerodynamic analysis. The development of a comprehensive structural analysis tool within the VSP environment will even enhance these capabilities for complex and multidisciplinary analysis of aircraft.

Chapter 5

Conclusion and Future Work

This study has been conducted with the motivation to eventually develop a suitable fidelity aeroelastic modeling within the multidisciplinary optimization framework. A low-order aerodynamic modeling method like Vortex-Lattice Method proves to be fit for conceptual analysis of aircraft, as it isn't computationally expensive and can be used for preliminary analysis. Coupling this with an open-source platform like OpenVSP, makes it a rapid and valuable analysis tool. The VSP environment also offers API integration with multiple structural, mathematical and aerodynamic analysis environments. This capability can be leveraged to further to increase fidelity and develop packages for detailed analysis such as modeling aeroelasticity. This will aid in incorporating flight dynamics in MDO in a quicker and reliable form.

In terms of analysis, sectional lift and drag coefficient distribution and its variation with Mach number and angle of attack have been presented in the study. These results are for cantilever and both SBW and TBW configurations, which have fairly similar configurations to aircraft configurations with medium range mission profile, having a 200-passenger capacity and a range of 3500NM. An increase in the aspect ratio demonstrates the increase in the lift-to-drag ratio. A comparison study for Δc_p has also been shown for analysis based on changes in configuration, Mach number and the angle of attack. It demonstrates the need to include the aerodynamic lift of the supporting members (strut and jury) for aerodynamic calculations. These results do account for the compressibility effects due to flow conditions of

the application. The derivatives obtained from this study show a good agreement with those obtained from the USM3D and FUN3D results in a superposition study [3]. The variations in derivatives are under 5% compared to the CFD results. As discussed earlier, the results also demonstrate a better agreement in terms of derivatives as compared to the superposition approach. With some additional considerations in modeling, the need to perform separate analyses for different components of aircraft and then perform post-processing to obtain the results can be eliminated. The user interface of OpenVSP and VSPAero allows for easier implementation of the methodology than scripted interfaces.

Despite, the demonstration of implementing the VLM through VSP efficiently, it has been observed that there are certain challenges and limitations within the environment. As the complexity of the aircraft configuration increases, additional considerations such as transonic and viscous effects discussed earlier can be applied. Additonally, VSPAero offers panel method implementation for aerodynamic modelling, which discretizes a three-dimensional geometry into a series of panels. This can be explored to overcome drawbacks of VLM in modeling non-lifting and blunt surfaces such as fuselage and engines. An external package to compute wave drag can be developed and integrated within this architecture to overcome the shortcoming wave drag computation for this application.

However, these tools still offer a rapid and sufficiently detailed aerodynamic analysis for MDO of complex TBW aircraft. Ultimately, the results obtained from these aerodynamic analyses will be coupled with structural finite-element methods to generate the flight dynamics model. The developers of OpenVSP have added some rudimentary structural modeling capability to the environment and are considering developing a capability to compute mode shapes and natural frequencies of the aircraft. This will open up the possibility of generating all the required data for flight dynamics modeling in an open-source software package, thereby, eliminating complex and expensive analysis tools.

Appendices

Appendix A

A.1 VSPAero GUI and Setup

The following figures demonstrate a detailed setup specified for OpenVSP models and VSPAero.

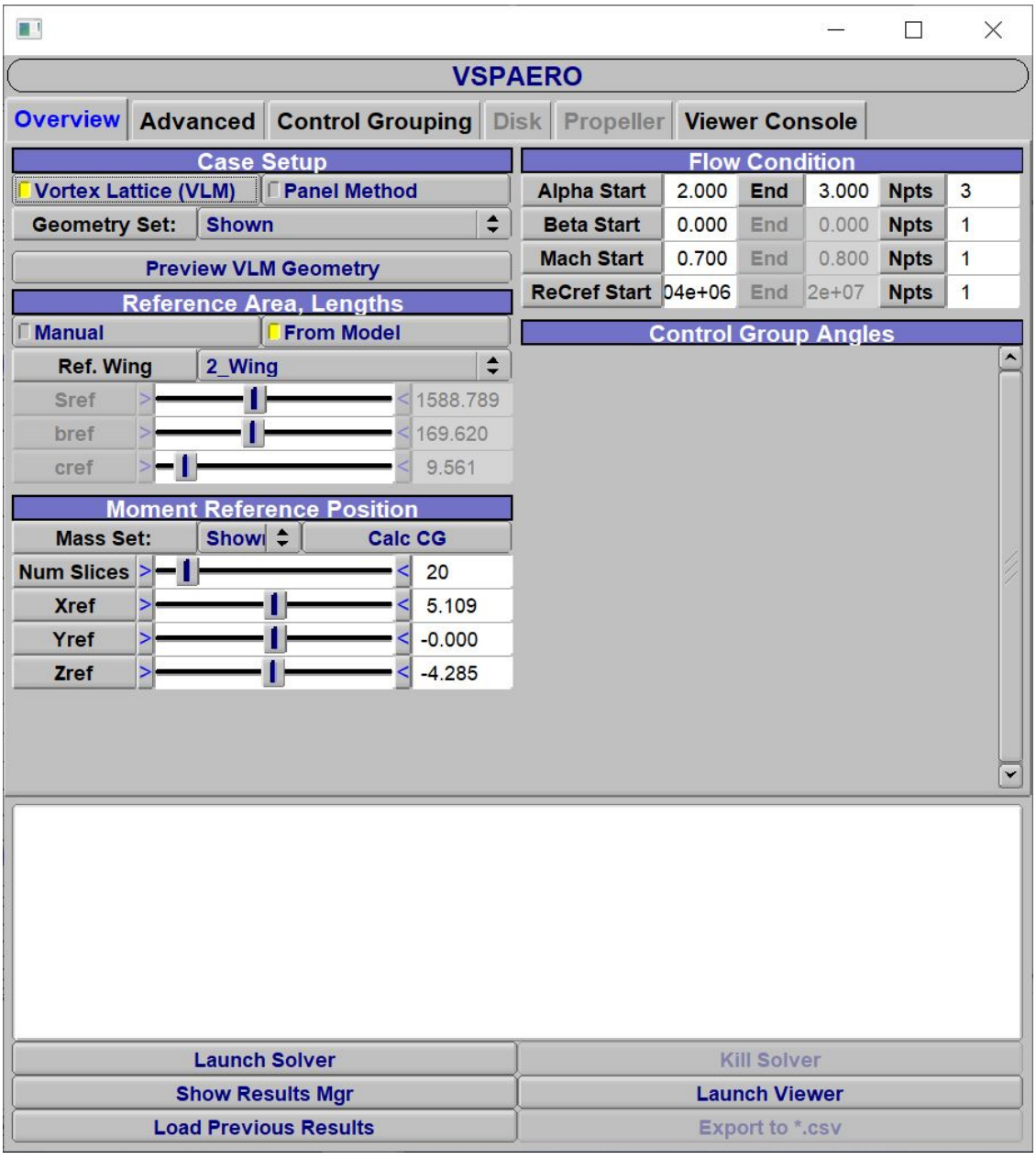

Figure A.1: VSPAero overview setup GUI

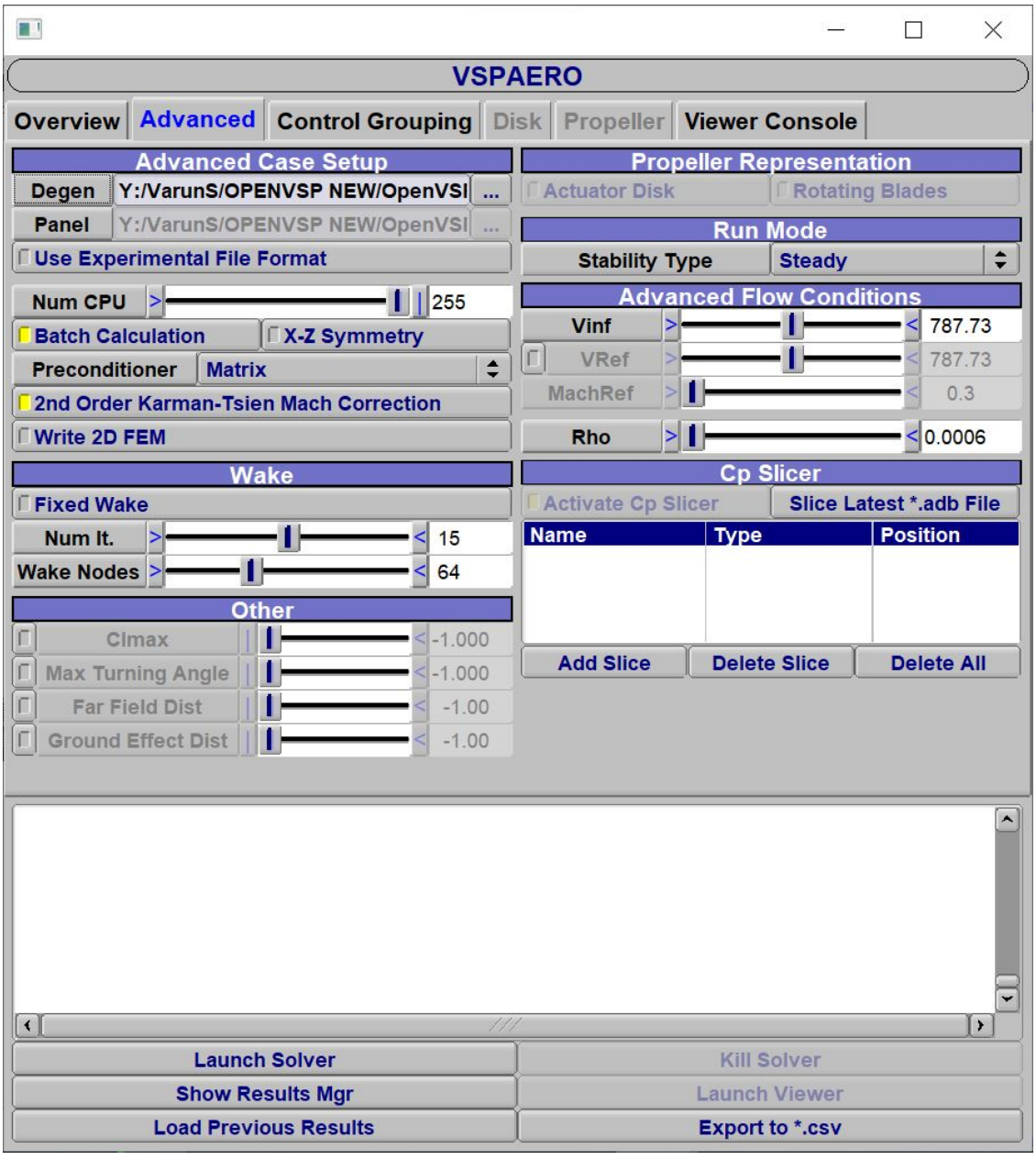

Figure A.2: VSPAero advanced setup GUI

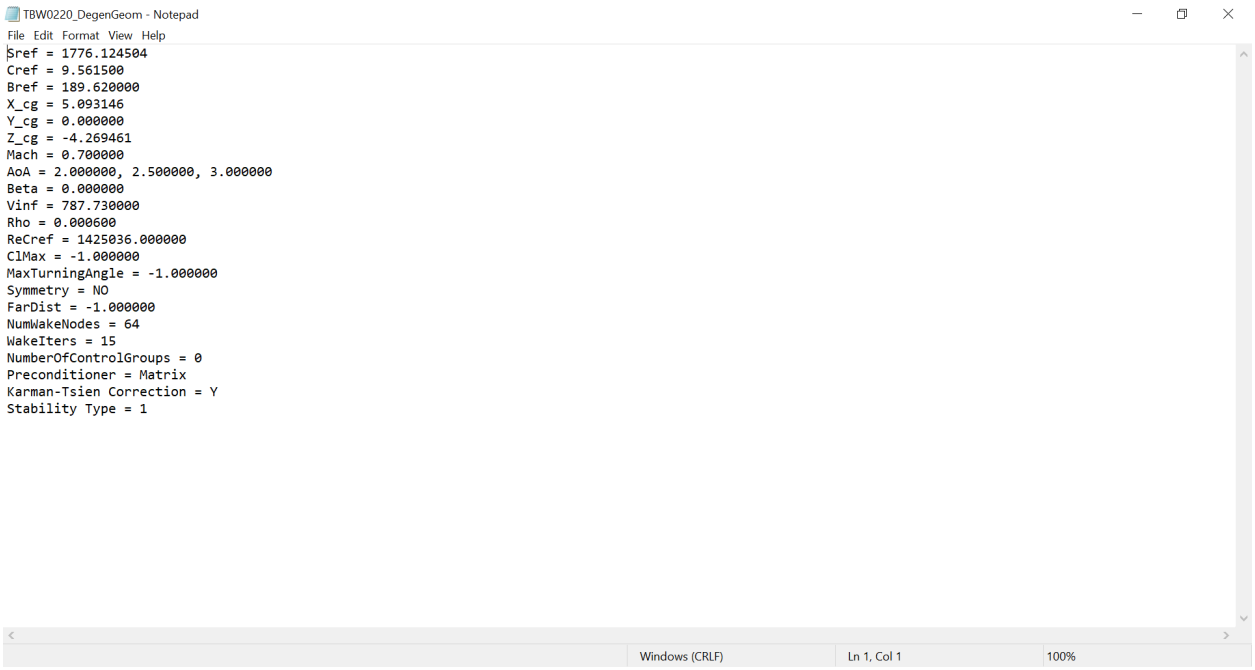

Figure A.3: VSPAero Setup and Inputs script file

Appendix B

B.1 Coefficients and Derivatives

Table B.1: Force Stability Derivatives for different aircraft configurations

	Configurations		
Derivatives	SBW	TBW-I	TBW-II
C_{Fx_α}	-0.0165	-1.0596	-0.7593
C_{Fx_β}	-0.90811	-0.0219	0.0059
C_{Fx_p}	-0.1713	0.2930	-0.1577
C_{Fx_q}	-0.6341	-1.1860	-0.6535
C_{Fx_r}	-0.0308	-0.0657	-0.0236
$C_{Fx_{M_\infty}}$	-0.0155	-0.0223	-0.04935
C_{Fx_u}	-0.0109	-0.0156	-0.0345
C_{Fy_α}	0.0970	0.0154	0.0207
C_{Fy_β}	-1.1152	-1.0533	125.790
C_{Fy_p}	-0.0592	-0.1430	63.0968
C_{Fy_q}	0.1227	0.0377	-0.0404
C_{Fy_r}	0.7672	0.7696	4.1421
$C_{Fy_{M_\infty}}$	0.0078	0.0055	0.0316
C_{Fy_u}	0.0055	0.0038	0.0213
C_{Fz_α}	9.6840	9.69511	9.845
C_{Fz_β}	-0.0168	-0.0075	-0.02706
C_{Fz_p}	0.0154	0.0231	-0.0125
C_{Fz_q}	4.6894	4.0981	4.1170
C_{Fz_r}	0.0459	0.0928	0.0446
$C_{Fz_{M_\infty}}$	1.055	1.2634	1.1091
C_{Fz_u}	0.7389	0.8844	0.0213

Unit for all derivatives is per rad, except for M_∞ and u

Table B.2: Moment Stability Derivatives for different aircraft configurations

	Configurations		
Derivatives	SBW	TBW-I	TBW-II
C_{Mx_α}	1.6496	-0.1665	-0.0013
C_{Mx_β}	-0.8259	-0.1214	-2.4494
C_{Mx_p}	0.9512	0.9647	-0.0836
C_{Mx_q}	-0.3437	-0.2293	-0.0033
C_{Mx_r}	-0.2054	-0.8679	-0.2259
$C_{Mx_{M_\infty}}$	-0.0256	-0.0223	-0.0002
C_{Mx_u}	-0.0148	-0.0179	-0.0001
C_{My_α}	-5090.389	519.2777	2.0913
C_{My_β}	-239.0355	333.7330	-1284.7955
C_{My_p}	99.9576	-296.4463	0.0575
C_{My_q}	1659.0391	569.9631	-85.2760
C_{My_r}	97.9410	-14989.64	-0.8666
$C_{My_{M_\infty}}$	107.2607	94.8922	-0.8762
C_{My_u}	75.0824	66.4245	-0.6133
C_{Mz_α}	-36.0011	4.1327	0.0182
C_{Mz_β}	25.0001	6.8773	8.9021
C_{Mz_p}	0.4960	0.4243	0.6715
C_{Mz_q}	8.3093	5.4899	0.0394
C_{Mz_r}	0.6691	16.7449	0.1110
$C_{Mz_{M_\infty}}$	0.5145	0.6280	0.0028
C_{Mz_u}	0.3601	0.4396	0.0020

Unit for all derivatives is per rad, except for M_∞ and u

```
****************************************************************************************************************************************************************************************************

# Name                 Value      Units
Sref_             1588.7893600 Lunit^2
Cref_                9.5615000 Lunit
Bref_              169.6200000 Lunit
Xcg_                 5.1094120 Lunit
Ycg_                -0.0000000 Lunit
Zcg_                -4.2847720 Lunit
Mach_                0.7000000 no_unit
AoA_                 2.0000000 deg
Beta_                0.0000000 deg
Rho_                 0.0006000 Munit/Lunit^3
Vinf_              787.7300000 Lunit/Tunit
Roll__Rate           0.0000000 rad/Tunit
Pitch_Rate           0.0000000 rad/Tunit
Yaw___Rate           0.0000000 rad/Tunit

#
Case                 Delta    Units          CFx          CFy          CFz          CMx          CMy          CMz           CL           CD           CS          CMl          CMm          CMn
#
Base_Aero            +0.000 n/a        -0.0105708   -0.0009410    0.3398306    0.0122651  -78.2971249   -0.3055326    0.3399925    0.0012955   -0.0009410   -0.0122651  -78.2971249    0.3055326
Alpha                +1.000 deg        -0.0238262   -0.0000091    0.5099505    0.0001365   -0.9164553   -0.0022578    0.5104986    0.0028952   -0.0000091   -0.0001365   -0.9164553    0.0022578
Beta                 +1.000 deg        -0.0117121   -0.0217217    0.3404282    0.0028515    4.6372625    0.0006269    0.3406296    0.0005548   -0.0217153   -0.0028515    4.6372625   -0.0006269
Roll__Rate           +1.000 rad/Tunit  -0.0290953   -0.0036297    0.3412137    0.0975140  -10.2397268    0.1700353    0.3420212   -0.0171694   -0.0036297   -0.0975140  -10.2397268   -0.1700353
Pitch_Rate           +1.000 rad/Tunit  -0.0147988   -0.0000038    0.3693425   -0.0000015   -0.4448236    0.0001194    0.3696340   -0.0018999   -0.0000038    0.0000015   -0.4448236   -0.0001194
Yaw___Rate           +1.000 rad/Tunit  -0.0140866    0.0797105    0.3441675   -0.0145653   -1.9154833   -0.0665408    0.3444494   -0.0020668    0.0797105    0.0145653   -1.9154833    0.0665408
Mach                 +0.100 no_unit    -0.0115885    0.0003263    0.4246868    0.0003683   -0.2759715   -0.0107861    0.4248325    0.0032399    0.0003263   -0.0003683   -0.2759715    0.0107861
#
#
#            Base     Derivative:
#            Aero         wrt          wrt          wrt          wrt          wrt          wrt          wrt
Coef         Total        Alpha        Beta         p            q            r            Mach         U
#              -          per          per          per          per          per          per          per
#              -          rad          rad          rad          rad          rad          M            u
#
CFx       -0.0105708   -0.7594760   -0.0653922   -0.1720585   -0.6966449   -0.0326550   -0.0101763   -0.0071234
CFy       -0.0009410    0.0533947   -1.1906471   -0.0249732    0.1544204    0.7491047    0.0126732    0.0088712
CFz        0.3398306    9.7471541    0.0342433    0.0128466    4.8627178    0.0402820    0.8485623    0.5939936
CMx        0.0122651   -0.6949191   -0.5393607    0.7918063   -2.0211786   -0.2492053   -0.1189679   -0.0832775
CMy      -78.2971249 4433.5867093 4751.7913627  632.1289262 12827.8185081  709.4459451  780.2115340  546.1480738
CMz       -0.3055326   17.3763733   17.5416517    4.4171571   50.3626510    2.2197979    2.9474651    2.0632256
CL         0.3399925    9.7692815    0.0365046    0.0188435    4.8840681    0.0413971    0.8484006    0.5938804
CD         0.0012955    0.0916553   -0.0424383   -0.1715054   -0.5265141   -0.0312293    0.0194442    0.0136110
CS        -0.0009410    0.0533947   -1.1902818   -0.0249732    0.1544204    0.7491047    0.0126732    0.0088712
CMl       -0.0122651    0.6949191    0.5393607   -0.7918063    2.0211786    0.2492053    0.1189679    0.0832775
CMm      -78.2971249 4433.5867093 4751.7913627  632.1289262 12827.8185081  709.4459451  780.2115340  546.1480738
CMn        0.3055326  -17.3763733  -17.5416517   -4.4171571  -50.3626510   -2.2197979   -2.9474651   -2.0632256
#
```

Figure B.1: Coefficients and Stability Derivatives for Strut-Braced Wing (SBW) configuration for α= 2 deg

```
****************************************************************************************************

# Name                  Value      Units
Sref_              1588.7893600 Lunit^2
Cref_                 9.5615000 Lunit
Bref_               169.6200000 Lunit
Xcg_                  5.1094120 Lunit
Ycg_                 -0.0000000 Lunit
Zcg_                 -4.2847720 Lunit
Mach_                 0.7000000 no_unit
AoA_                  2.5000000 deg
Beta_                 0.0000000 deg
Rho_                  0.0006000 Munit/Lunit^3
Vinf_               787.7300000 Lunit/Tunit
Roll__Rate            0.0000000 rad/Tunit
Pitch_Rate            0.0000000 rad/Tunit
Yaw___Rate            0.0000000 rad/Tunit

#
Case                  Delta    Units          CFx         CFy         CFz         CMx         CMy         CMz          CL          CD          CS         CMl         CMm         CMn
#
Base_Aero             +0.000 n/a          -0.0165387  -0.0007461   0.4250507   0.0020850 -10.4727520  -0.0503477   0.4253675   0.0020175  -0.0007461  -0.0020850 -10.4727520   0.0503477
Alpha                 +1.000 deg          -0.0323883   0.0009470   0.5940692   0.0308764 -99.3167823  -0.6786849   0.5949384   0.0039392   0.0009470  -0.0308764 -99.3167823   0.6786849
Beta                  +1.000 deg          -0.0164888  -0.0202113   0.4247574  -0.0123290 -14.6447085   0.3859867   0.4250724   0.0024069  -0.0201723   0.0123290 -14.6447085  -0.3859867
Roll__Rate            +1.000 rad/Tunit    -0.0349823  -0.0071236   0.4267117   0.1044989   0.2890644   0.0030530   0.4278315  -0.0163361  -0.0071236  -0.1044989   0.2890644  -0.0030530
Pitch_Rate            +1.000 rad/Tunit    -0.0203873  -0.0000010   0.4535108  -0.0000011  -0.4040081   0.0000818   0.4539685  -0.0005861  -0.0000010   0.0000011  -0.4040081  -0.0000818
Yaw___Rate            +1.000 rad/Tunit    -0.0198544   0.0818616   0.4299927  -0.0200313   0.0719439   0.0216963   0.4304495  -0.0010795   0.0818616   0.0200313   0.0719439  -0.0216963
Mach                  +0.100 no_unit      -0.0180944   0.0000369   0.5306134  -0.0000273   0.2533181   0.0011032   0.5308976   0.0050678   0.0000369   0.0000273   0.2533181  -0.0011032
#
#
#            Base      Derivative:
#            Aero         wrt          wrt          wrt          wrt          wrt          wrt          wrt
Coef         Total        Alpha        Beta         p            q            r            Mach         U
#            -            per          per          per          per          per          per          per
#            -            rad          rad          rad          rad          rad          M            u
#
CFx      -0.0165387   -0.9081148    0.0028565   -0.1713075   -0.6341445   -0.0307968   -0.0155571   -0.0108900
CFy      -0.0007461    0.0970031   -1.1152750   -0.0592354    0.1227735    0.7672743    0.0078294    0.0054806
CFz       0.4250507    9.6840490   -0.0168045    0.0154279    4.6894136    0.0459025    1.0556270    0.7389389
CMx       0.0020850    1.6496256   -0.8258617    0.9512381   -0.3437345   -0.2054204   -0.0211225   -0.0147857
CMy     -10.4727520 -5090.3890301 -239.0355528   99.9576185 1659.0391912   97.9409653  107.2607008   75.0824906
CMz      -0.0503477  -36.0010788   25.0001241    0.4959947    8.3093328    0.6691575    0.5145093    0.3601565
CL        0.4253675    9.7156960   -0.0169131    0.0228856    4.7126113    0.0472021    1.0553008    0.7387106
CD        0.0020175    0.1101043    0.0223131   -0.1704715   -0.4289917   -0.0287652    0.0305035    0.0213524
CS       -0.0007461    0.0970031   -1.1130443   -0.0592354    0.1227735    0.7672743    0.0078294    0.0054806
CMl      -0.0020850   -1.6496256    0.8258617   -0.9512381    0.3437345    0.2054204    0.0211225    0.0147857
CMm     -10.4727520 -5090.3890301 -239.0355528   99.9576185 1659.0391912   97.9409653  107.2607008   75.0824906
CMn       0.0503477   36.0010788  -25.0001241   -0.4959947   -8.3093328   -0.6691575   -0.5145093   -0.3601565
#
```

Figure B.2: Coefficients and Stability Derivatives for Strut-Braced Wing (SBW) configuration for α= 2.5 deg

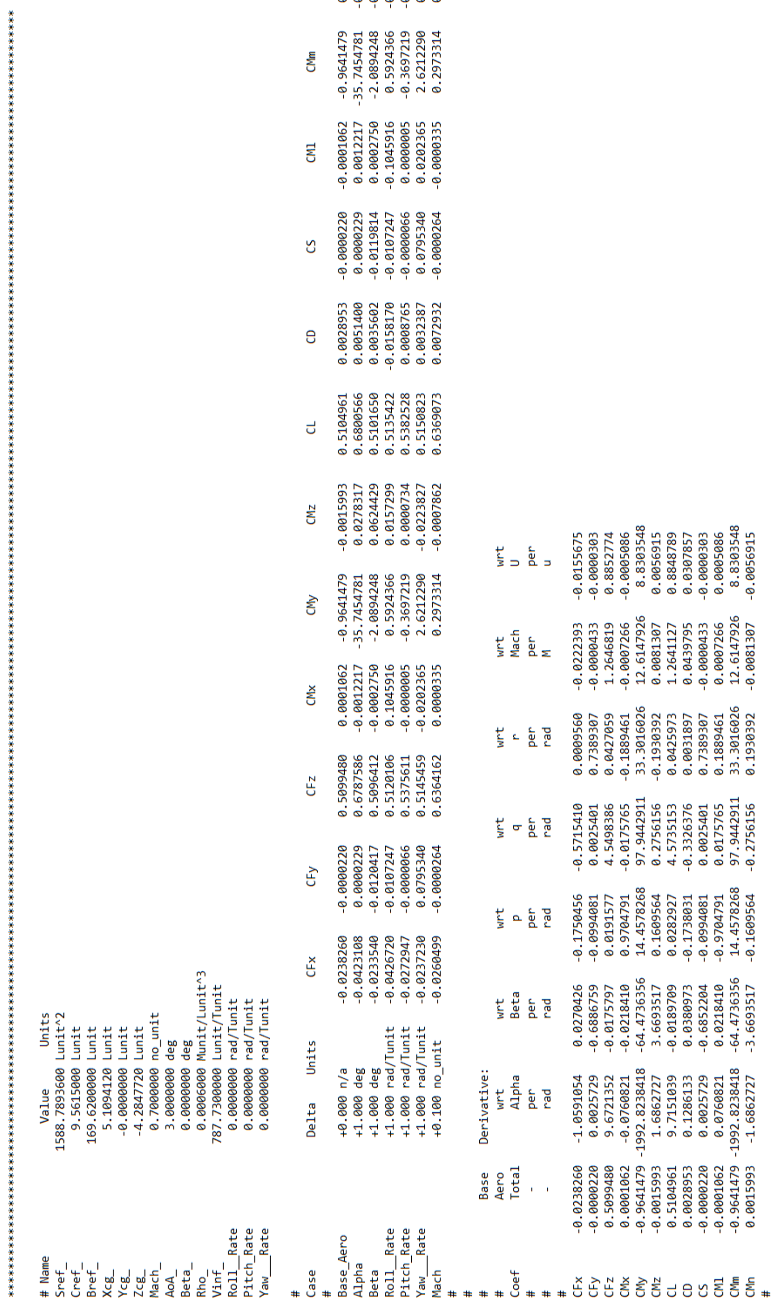

```
******************************************************************************************************************************************************************

# Name                  Value      Units
Sref_               1588.7893600 Lunit^2
Cref_                  9.5615000 Lunit
Bref_                169.6200000 Lunit
Xcg_                   5.1094120 Lunit
Ycg_                  -0.0000000 Lunit
Zcg_                  -4.2847720 Lunit
Mach_                  0.7000000 no_unit
AoA_                   3.0000000 deg
Beta_                  0.0000000 deg
Rho_                   0.0006000 Munit/Lunit^3
Vinf_                787.7300000 Lunit/Tunit
Roll__Rate             0.0000000 rad/Tunit
Pitch_Rate             0.0000000 rad/Tunit
Yaw___Rate             0.0000000 rad/Tunit

#
Case                   Delta    Units          CFx          CFy          CFz          CMx          CMy          CMz           CL           CD           CS          CMl          CMm          CMn
#
Base_Aero              +0.000 n/a          -0.0238260   -0.0000220    0.5099480    0.0001062   -0.9641479   -0.0015993    0.5104961    0.0028953   -0.0000220   -0.0001062   -0.9641479    0.0015993
Alpha                  +1.000 deg          -0.0423108    0.0000229    0.6787586   -0.0012217  -35.7454781    0.0278317    0.6800566    0.0051400    0.0000229    0.0012217  -35.7454781   -0.0278317
Beta                   +1.000 deg          -0.0233540   -0.0120417    0.5096412   -0.0002750   -2.0894248    0.0624429    0.5101650    0.0035602   -0.0119814    0.0002750   -2.0894248   -0.0624429
Roll__Rate             +1.000 rad/Tunit    -0.0426720   -0.0107247    0.5120106    0.1045916    0.5924366    0.0157299    0.5135422   -0.0158170   -0.0107247   -0.1045916    0.5924366   -0.0157299
Pitch_Rate             +1.000 rad/Tunit    -0.0272947   -0.0000066    0.5375611   -0.0000005   -0.3697219    0.0000734    0.5382528    0.0008765   -0.0000066    0.0000005   -0.3697219   -0.0000734
Yaw___Rate             +1.000 rad/Tunit    -0.0237230    0.0795340    0.5145459   -0.0202365    2.6212290   -0.0223827    0.5150823    0.0032387    0.0795340    0.0202365    2.6212290    0.0223827
Mach                   +0.100 no_unit      -0.0260499   -0.0000264    0.6364162    0.0000335    0.2973314   -0.0007862    0.6369073    0.0072932   -0.0000264   -0.0000335    0.2973314    0.0007862
#
#
#              Base    Derivative:
#              Aero         wrt          wrt          wrt          wrt          wrt          wrt          wrt
Coef           Total        Alpha        Beta         p            q            r            Mach         U
#              -            per          per          per          per          per          per          per
#              -            rad          rad          rad          rad          rad          M            u
#
CFx      -0.0238260   -1.0591054    0.0270426   -0.1750456   -0.5715410    0.0009560   -0.0222393   -0.0155675
CFy      -0.0000220    0.0025729   -0.6886759   -0.0994081    0.0025401    0.7389307   -0.0000433   -0.0000303
CFz       0.5099480    9.6721352   -0.0175797    0.0191577    4.5498386    0.0427059    1.2646819    0.8852774
CMx       0.0001062   -0.0760821   -0.0218410    0.9704791   -0.0175765   -0.1889461   -0.0007266   -0.0005086
CMy      -0.9641479 -1992.8238418  -64.4736356   14.4578268   97.9442911   33.3016026   12.6147926    8.8303548
CMz      -0.0015993    1.6862727    3.6693517    0.1609564    0.2756156   -0.1930392    0.0081307    0.0056915
CL        0.5104961    9.7151039   -0.0189709    0.0282927    4.5735153    0.0425973    1.2641127    0.8848789
CD        0.0028953    0.1286133    0.0380973   -0.1738031   -0.3326376    0.0031897    0.0439795    0.0307857
CS       -0.0000220    0.0025729   -0.6852204   -0.0994081    0.0025401    0.7389307   -0.0000433   -0.0000303
CMl      -0.0001062    0.0760821    0.0218410   -0.9704791    0.0175765    0.1889461    0.0007266    0.0005086
CMm      -0.9641479 -1992.8238418  -64.4736356   14.4578268   97.9442911   33.3016026   12.6147926    8.8303548
CMn       0.0015993   -1.6862727   -3.6693517   -0.1609564   -0.2756156    0.1930392   -0.0081307   -0.0056915
#
```

Figure B.3: Coefficients and Stability Derivatives for Strut-Braced Wing (SBW) configuration for α= 3 deg

```
*****************************************************************************************************************

# Name                Value      Units
Sref_             1588.7893600 Lunit^2
Cref_                9.5615000 Lunit
Bref_              169.6200000 Lunit
Xcg_                 5.1068110 Lunit
Ycg_                 0.0000000 Lunit
Zcg_                -4.2839950 Lunit
Mach_                0.7000000 no_unit
AoA_                 2.0000000 deg
Beta_                0.0000000 deg
Rho_                 0.0006000 Munit/Lunit^3
Vinf_              461.9660000 Lunit/Tunit
Roll__Rate           0.0000000 rad/Tunit
Pitch_Rate           0.0000000 rad/Tunit
Yaw___Rate           0.0000000 rad/Tunit

#
Case                 Delta    Units         CFx         CFy         CFz         CMx         CMy         CMz          CL          CD          CS         CMl         CMm         CMn
#
Base_Aero            +0.000 n/a        -0.0105713  -0.0002387   0.3399170   0.0020850  -14.5879521  -0.0514366   0.3400788   0.0012981  -0.0002387  -0.0020850  -14.5879521   0.0514366
Alpha                +1.000 deg        -0.0238040  -0.0004917   0.5097275   0.0003179   -2.8972900  -0.0065557   0.5102747   0.0029057  -0.0004917  -0.0003179   -2.8972900   0.0065557
Beta                 +1.000 deg        -0.2163265   0.0769850   0.4542155  -0.5001442 78476.4111689  11.6549158   0.4614885  -0.2016559   0.0734768   0.5001442 78476.4111689 -11.6549158
Roll__Rate           +1.000 rad/Tunit  -0.0581840  -0.0363529   0.3403556   0.1783048 -1064.7595948   0.0195787   0.3421788  -0.0462703  -0.0363529  -0.1783048 -1064.7595948  -0.0195787
Pitch_Rate           +1.000 rad/Tunit  -0.0241477  -0.0000177   0.3848403  -0.0001377   -1.7647662   0.0035172   0.3854486  -0.0107023  -0.0000177   0.0001377   -1.7647662  -0.0035172
Yaw___Rate           +1.000 rad/Tunit  -0.0182624   0.1296523   0.3505633   0.0139615  -25.5135421  -1.1079576   0.3509871  -0.0060168   0.1296523  -0.0139615  -25.5135421   1.1079576
Mach                 +0.100 no_unit    -0.0115793   0.0000569   0.4244030  -0.0000687    0.2308824   0.0045068   0.4245486   0.0032392   0.0000569   0.0000687    0.2308824  -0.0045068
#
#
#             Base    Derivative:
#             Aero        wrt           wrt           wrt           wrt           wrt           wrt           wrt
Coef          Total       Alpha         Beta          p             q             r             Mach          U
#               -         per           per           per           per           per           per           per
#               -         rad           rad           rad           rad           rad           M             u
#
CFx       -0.0105713   -0.7581766  -11.7889099   -0.2593499   -1.3118996   -0.0418941   -0.0100802   -0.0070561
CFy       -0.0002387   -0.0144957    4.4245926   -0.1967168    0.0213555    0.7075252    0.0029563    0.0020694
CFz        0.3399170    9.7294286    6.5488252    0.0023889    4.3409611    0.0579911    0.8448606    0.5914024
CMx        0.0020850   -0.1012485  -28.7756192    0.9598812   -0.2147874    0.0646917   -0.0215374   -0.0150762
CMy      -14.5879521  669.8257356 4497203.9150172 -5720.3583666 1239.1101616  -59.5124526  148.1883449  103.7318414
CMz       -0.0514366    2.5714865  670.7247248    0.3868253    5.3102091   -5.7549441    0.5594333    0.3916033
CL         0.3400788    9.7515090    6.9562628    0.0114386    4.3841014    0.0594179    0.8446978    0.5912884
CD         0.0012981    0.0921115  -11.6284106   -0.2591085   -1.1596031   -0.0398447    0.0194112    0.0135878
CS        -0.0002387   -0.0144957    4.2235881   -0.1967168    0.0213555    0.7075252    0.0029563    0.0020694
CMl       -0.0020850    0.1012485   28.7756192   -0.9598812    0.2147874   -0.0646917    0.0215374    0.0150762
CMm      -14.5879521  669.8257356 4497203.9150172 -5720.3583666 1239.1101616  -59.5124526  148.1883449  103.7318414
CMn        0.0514366   -2.5714865 -670.7247248   -0.3868253   -5.3102091    5.7549441   -0.5594333   -0.3916033
#
#
```

Figure B.4: Coefficients and Stability Derivatives for Truss-Braced Wing (TBW) configuration for α= 2 deg

```
*************************************************************************************************************************************************

# Name                 Value      Units
Sref_              1588.7893600 Lunit^2
Cref_                 9.5615000 Lunit
Bref_               169.6200000 Lunit
Xcg_                  5.1068110 Lunit
Ycg_                  0.0000000 Lunit
Zcg_                 -4.2839950 Lunit
Mach_                 0.7000000 no_unit
AoA_                  2.5000000 deg
Beta_                 0.0000000 deg
Rho_                  0.0006000 Munit/Lunit^3
Vinf_               461.9660000 Lunit/Tunit
Roll__Rate            0.0000000 rad/Tunit
Pitch_Rate            0.0000000 rad/Tunit
Yaw___Rate            0.0000000 rad/Tunit

#
Case                    Delta    Units          CFx         CFy         CFz         CMx         CMy         CMz          CL          CD          CS         CMl         CMm         CMn
#
Base_Aero               +0.000 n/a          -0.0165284  -0.0009803   0.4248743   0.0025352  -9.2587908  -0.0615459   0.4251909   0.0020201  -0.0009803  -0.0025352  -9.2587908   0.0615459
Alpha                   +1.000 deg          -0.0323903   0.0000006   0.5943529  -0.0003542  -0.1956861   0.0105826   0.5952217   0.0039544   0.0000006   0.0003542  -0.1956861  -0.0105826
Beta                    +1.000 deg          -0.0162923  -0.0207582   0.4247607   0.0004151  -3.4340530   0.0584865   0.4250671   0.0026129  -0.0207157  -0.0004151  -3.4340530  -0.0584865
Roll__Rate              +1.000 rad/Tunit    -0.0701745  -0.0092375   0.4286113   0.1796414 -63.6818596   0.0173915   0.4312643  -0.0514120  -0.0092375  -0.1796414 -63.6818596  -0.0173915
Pitch_Rate              +1.000 rad/Tunit    -0.0294526   0.0000359   0.4685017   0.0001619  -3.3604102  -0.0047326   0.4693405  -0.0089889   0.0000359  -0.0001619  -3.3604102   0.0047326
Yaw___Rate              +1.000 rad/Tunit    -0.0092953   0.1462418   0.4346722  -0.1567985 -2761.1314028   3.0125761   0.4346639   0.0096737   0.1462418   0.1567985 -2761.1314028  -3.0125761
Mach                    +0.100 no_unit      -0.0180817   0.0000238   0.5302682  -0.0000286   0.2304311   0.0012555   0.5305522   0.0050654   0.0000238   0.0000286   0.2304311  -0.0012555
#
#
#             Base     Derivative:
#             Aero        wrt          wrt          wrt          wrt          wrt          wrt          wrt
Coef          Total       Alpha        Beta         p            q            r            Mach         U
#              -          per          per          per          per          per          per          per
#              -          rad          rad          rad          rad          rad          M            u
#
CFx        -0.0165284  -0.9088235   0.0135242  -0.2922141  -1.2488762   0.0393991  -0.0155334  -0.0108734
CFy        -0.0009803   0.0562000  -1.1331899  -0.0449775   0.0981962   0.8019287   0.0100404   0.0070283
CFz         0.4248743   9.7104083  -0.0065108   0.0203556   4.2157277   0.0533697   1.0539389   0.7377573
CMx         0.0025352  -0.1655499  -0.1214717   0.9647100  -0.2293256  -0.8679015  -0.0256376  -0.0179463
CMy        -9.2587908 519.2777561 333.7329631 -296.4462609 569.9631422 -14989.6425314  94.8922191  66.4245533
CMz        -0.0615459   4.1326564   6.8773463   0.4299775   5.4898876  16.7449573   0.6280136   0.4396095
CL          0.4251909   9.7420484  -0.0070945   0.0330825   4.2661905   0.0516003   1.0536134   0.7375294
CD          0.0020201   0.1108294   0.0339648  -0.2910481  -1.0638001   0.0416896   0.0304535   0.0213175
CS         -0.0009803   0.0562000  -1.1307579  -0.0449775   0.0981962   0.8019287   0.0100404   0.0070283
CMl        -0.0025352   0.1655499   0.1214717  -0.9647100   0.2293256   0.8679015   0.0256376   0.0179463
CMm        -9.2587908 519.2777561 333.7329631 -296.4462609 569.9631422 -14989.6425314  94.8922191  66.4245533
CMn         0.0615459  -4.1326564  -6.8773463  -0.4299775  -5.4898876 -16.7449573  -0.6280136  -0.4396095
#
#
```

Figure B.5: Coefficients and Stability Derivatives for Truss-Braced Wing (TBW) configuration for α= 2.5 deg

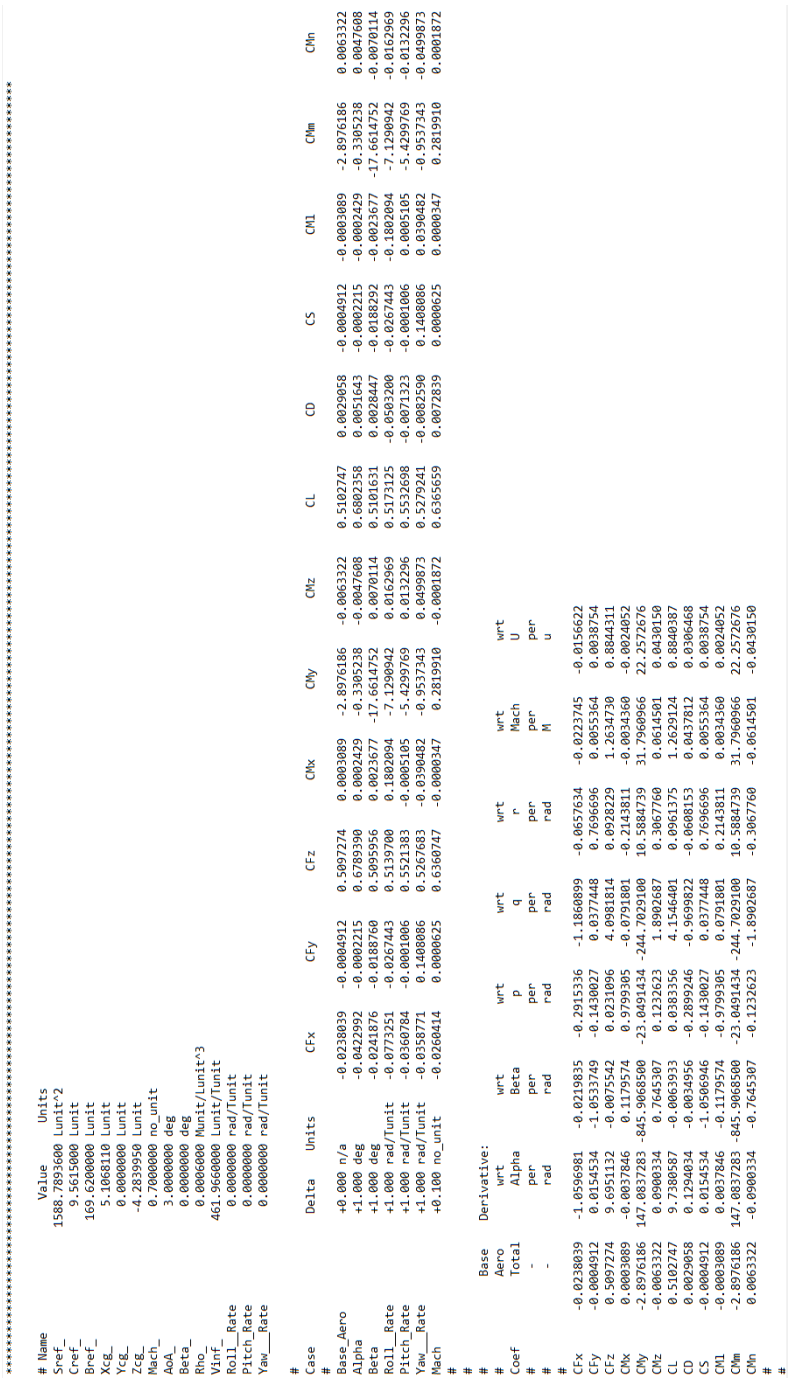

```
# Name          Value      Units
# Sref_       1588.7893600 Lunit^2
# Cref_          9.5615000 Lunit
# Bref_        169.6200000 Lunit
# Xcg_           5.1068110 Lunit
# Ycg_           0.0000000 Lunit
# Zcg_          -4.2839950 Lunit
# Mach_          0.7000000 no_unit
# AoA_           3.0000000 deg
# Beta_          0.0000000 deg
# Rho_           0.0006000 Munit/Lunit^3
# Vinf_        461.9660000 Lunit/Tunit
# Roll_Rate      0.0000000 rad/Tunit
# Pitch_Rate     0.0000000 rad/Tunit
# Yaw__Rate      0.0000000 rad/Tunit
#
#  Case          Delta   Units       CFx        CFy        CFz        CMx        CMy        CMz        CL         CD         CS         CM1        CMm        CMn
#
#  Base_Aero     +0.000 n/a       -0.0238039 -0.0004912  0.5097274  0.0003089 -2.8976186 -0.0063322  0.5102747  0.0029058 -0.0004912 -0.0003089 -2.8976186  0.0063322
#  Alpha         +1.000 deg       -0.0422992 -0.0002215  0.6789390  0.0002429 -0.3305238 -0.0047608  0.6802358  0.0051643 -0.0002215 -0.0002429 -0.3305238  0.0047608
#  Beta          +1.000 deg       -0.0241876 -0.0188760  0.5095956  0.0023677 -17.6614752  0.0070114  0.5101631  0.0028447 -0.0188292 -0.0023677 -17.6614752 -0.0070114
#  Roll_Rate     +1.000 rad/Tunit  -0.0773251 -0.0267443  0.5139700  0.1802094 -7.1290942  0.0162969  0.5173125 -0.0503200 -0.0267443 -0.1802094 -7.1290942 -0.0162969
#  Pitch_Rate    +1.000 rad/Tunit  -0.0360784 -0.0001006  0.5221383 -0.0005105 -5.4299769  0.0132296  0.5532698 -0.0071323 -0.0001006  0.0005105 -5.4299769 -0.0132296
#  Yaw__Rate     +1.000 rad/Tunit  -0.0358771  0.1408086  0.5267683 -0.0396482 -0.9537343  0.0499873  0.5279241 -0.0082590  0.1408086  0.0396482 -0.9537343 -0.0499873
#  Mach          +0.100 no_unit    -0.0260414  0.0000625  0.6360747 -0.0000347  0.2819910 -0.0001872  0.6365659  0.0072839  0.0000625  0.0000347  0.2819910 -0.0001872
#
#
#                Base   Derivative:
#                Aero        wrt        wrt        wrt        wrt        wrt        wrt
#  Coef          Total        Alpha      Beta       p          q          r          Mach       U
#  #             -            per        per        per        per        per        per        per
#  #             -            rad        rad        rad        rad        rad        M          u
#
#  CFx        -0.0238039  -1.0596981  -0.0219835  -0.2915336  -1.1860899  -0.0657634  -0.0223745  -0.0156622
#  CFy        -0.0004912   0.0154534  -1.0533749  -0.1430027   0.0377448   0.7696696   0.0055364   0.0038754
#  CFz         0.5097274   9.6951132  -0.0075542   0.0231096   4.0981814   0.0928229   1.2634730   0.8843311
#  CMx         0.0003089  -0.0037846   0.1179574   0.9799305  -0.0791801  -0.2143811  -0.0034360  -0.0024052
#  CMy        -2.8976186 147.0837283 -845.9068500 -23.0491434 -244.7029100 10.5884739  31.7960966  22.2572676
#  CMz        -0.0063322  -0.0900334   0.7645307   0.1232623   1.8902687  -0.3067760   0.0614501   0.0430150
#  CL          0.5102747   9.7380587  -0.0063933   0.0383356   4.1546401   0.0961375   1.2629124   0.8840387
#  CD          0.0029058   0.1294034  -0.0034956  -0.2899246  -0.9659822  -0.0608153   0.0437812   0.0306468
#  CS         -0.0004912   0.0154534  -1.0506946  -0.1430027   0.0377448   0.7696696   0.0055364   0.0038754
#  CM1        -0.0003089  -0.0037846  -0.1179574  -0.9799305   0.0791801   0.2143811   0.0034360   0.0024052
#  CMm        -2.8976186 147.0837283 -845.9068500 -23.0491434 -244.7029100 10.5884739  31.7960966  22.2572676
#  CMn         0.0063322  -0.0900334  -0.7645307  -0.1232623  -1.8902687  -0.3067760  -0.0614501  -0.0430150
#
#
```

Figure B.6: Coefficients and Stability Derivatives for Truss-Braced Wing (TBW) configuration for α= 3 deg

```
*****************************************************************************************************************************

# Name               Value      Units
Sref_            1776.1245040 Lunit^2
Cref_               9.5615000 Lunit
Bref_             189.6200000 Lunit
Xcg_                5.0931460 Lunit
Ycg_                0.0000000 Lunit
Zcg_               -4.2694610 Lunit
Mach_               0.7000000 no_unit
AoA_                2.0000000 deg
Beta_               0.0000000 deg
Rho_                0.0006000 Munit/Lunit^3
Vinf_             787.7300000 Lunit/Tunit
Roll__Rate          0.0000000 rad/Tunit
Pitch_Rate          0.0000000 rad/Tunit
Yaw___Rate          0.0000000 rad/Tunit

#
Case              Delta    Units         CFx          CFy          CFz          CMx          CMy          CMz          CL           CD           CS           CMl          CMm          CMn
#
Base_Aero         +0.000 n/a        -0.0088374   -0.0001446    0.3450047   -0.0000318   -0.7164440    0.0022225    0.3451030    0.0032084   -0.0001446    0.0000318   -0.7164440   -0.0022225
Alpha             +1.000 deg        -0.0198929   -0.0003323    0.5174379   -0.0000581    0.2222682    0.0020003    0.5177699    0.0072150   -0.0003323    0.0000581    0.2222682   -0.0020003
Beta              +1.000 deg        -0.1015040    1.5720851    0.4017901   -0.6025978 34688.4436717   13.5527789    0.4050878   -0.1148433    1.5703200    0.6025978 34688.4436717  -13.5527789
Roll__Rate        +1.000 rad/Tunit  -0.0281679    6.0820139    0.3464043    0.0158835    0.0381875   -0.0631216    0.3471763   -0.0160614    6.0820139   -0.0158835    0.0381875    0.0631216
Pitch_Rate        +1.000 rad/Tunit  -0.0130044   -0.0000090    0.3708245    0.0000003   -0.3805991   -0.0000013    0.3710525   -0.0000549   -0.0000090   -0.0000003   -0.3805991    0.0000013
Yaw___Rate        +1.000 rad/Tunit   0.0865555    0.7407349    0.2880326    0.3306291 -199540.5581926   -9.1222016    0.2848364    0.0965550    0.7407349   -0.3306291 -199540.5581926    9.1222016
Mach              +0.100 no_unit    -0.0119958   -0.0000340    0.4337587    0.0000057    0.1612151   -0.0001326    0.4339131    0.0031494   -0.0000340   -0.0000057    0.1612151    0.0001326
#
#
#            Base     Derivative:
#            Aero        wrt          wrt          wrt          wrt          wrt          wrt          wrt
Coef         Total       Alpha        Beta         p            q            r            Mach         U
#             -          per          per          per          per          per          per          per
#             -          rad          rad          rad          rad          rad          M            u
#
CFx      -0.0088374   -0.6334298   -5.3094050   -0.1606076   -0.6866055    0.7925736   -0.0315840   -0.0221088
CFy      -0.0001446   -0.0107556   90.0821439   50.5336853    0.0223306    6.1556059    0.0011054    0.0007738
CFz       0.3450047    9.8796991    3.2535643    0.0116286    4.2543639   -0.4733531    0.8875402    0.6212782
CMx      -0.0000318   -0.0015102  -34.5244980    0.1322325    0.0052862    2.7472997    0.0003749    0.0002624
CMy      -0.7164440   53.7842621 1987542.8829794    6.2698652   55.3375729 -1657879.1218289    8.7765917    6.1436142
CMz       0.0022225   -0.0127267  776.3898578   -0.5429118   -0.3664138  -75.8103846   -0.0235501   -0.0164851
CL        0.3451030    9.8930906    3.4368779    0.0172267    4.2757344   -0.5007251    0.8881018    0.6216713
CD        0.0032084    0.2295591   -6.7638654   -0.1601039   -0.5377121    0.7755710   -0.0005901   -0.0004131
CS       -0.0001446   -0.0107556   89.9810098   50.5336853    0.0223306    6.1556059    0.0011054    0.0007738
CMl       0.0000318    0.0015102   34.5244980   -0.1322325   -0.0052862   -2.7472997   -0.0003749   -0.0002624
CMm      -0.7164440   53.7842621 1987542.8829794    6.2698652   55.3375729 -1657879.1218289    8.7765917    6.1436142
CMn      -0.0022225    0.0127267 -776.3898578    0.5429118    0.3664138   75.8103846    0.0235501    0.0164851
#
```

Figure B.7: Coefficients and Stability Derivatives for Truss-Braced Wing (TBW-II) configuration for α= 2 deg

****

# Name	Value	Units
Sref_	1776.1245040	Lunit^2
Cref_	9.5615000	Lunit
Bref_	189.6200000	Lunit
Xcg_	5.0931460	Lunit
Ycg_	0.0000000	Lunit
Zcg_	-4.2694610	Lunit
Mach_	0.7000000	no_unit
AoA_	2.5000000	deg
Beta_	0.0000000	deg
Rho_	0.0006000	Munit/Lunit^3
Vinf_	787.7300000	Lunit/Tunit
Roll__Rate	0.0000000	rad/Tunit
Pitch_Rate	0.0000000	rad/Tunit
Yaw___Rate	0.0000000	rad/Tunit

Case	Delta	Units	CFx	CFy	CFz	CMx	CMy	CMz	CL	CD	CS	CMl	CMm	CMn
Base_Aero	+0.000	n/a	-0.0138129	-0.0002603	0.4313232	0.0000203	0.1759132	-0.0002348	0.4315152	0.0050143	-0.0002603	-0.0000203	0.1759132	0.0002348
Alpha	+1.000	deg	-0.0270664	0.0001016	0.6031558	-0.0000020	0.2124140	0.0000825	0.6036831	0.0098059	0.0001016	0.0000020	0.2124140	-0.0000825
Beta	+1.000	deg	-0.0137101	2.1951881	0.4308509	-0.0427301	-22.2479943	0.1551362	0.4310388	-0.0332157	2.1949427	0.0427301	-22.2479943	-0.1551362
Roll__Rate	+1.000	rad/Tunit	-0.0328012	7.5939825	0.4328281	-0.0100438	0.1828424	-0.0810526	0.4338469	-0.0138903	7.5939825	0.0100438	0.1828424	0.0810526
Pitch_Rate	+1.000	rad/Tunit	-0.0177795	-0.0000146	0.4563096	0.0000005	-0.3416289	0.0000047	0.4566508	0.0021414	-0.0000146	-0.0000005	-0.3416289	-0.0000047
Yaw___Rate	+1.000	rad/Tunit	-0.0166583	0.4982800	0.4366989	-0.0271748	0.0716061	0.0131280	0.4370099	0.0024061	0.4982800	0.0271748	0.0716061	-0.0131280
Mach	+0.100	no_unit	-0.0187487	0.0000562	0.5422342	-0.0000024	0.0882936	0.0000473	0.5425359	0.0049211	0.0000562	0.0000024	0.0882936	-0.0000473

Coef	Base Aero Total (-)	Derivative: wrt Alpha per rad	wrt Beta per rad	wrt p per rad	wrt q per rad	wrt r per rad	wrt Mach per M	wrt U per u
CFx	-0.0138129	-0.7593679	0.0058921	-0.1577642	-0.6535700	-0.0236410	-0.0493576	-0.0345503
CFy	-0.0002603	0.0207357	125.7899546	63.0968560	0.0404920	4.1421282	0.0031648	0.0022153
CFz	0.4313232	9.8452831	-0.0270626	0.0125031	4.1170383	0.0446639	1.1091100	0.7763770
CMx	0.0000203	-0.0012766	-2.4494158	-0.0836177	-0.0032620	-0.2259507	-0.0002269	-0.0001589
CMy	0.1759132	2.0913376	-1284.7955285	0.0575709	-85.2760422	-0.8666373	-0.8761960	-0.6133372
CMz	-0.0002348	0.0181796	8.9021018	-0.6714757	0.0394540	0.1110249	0.0028209	0.0019746
CL	0.4315152	9.8644984	-0.0272939	0.0193728	4.1416281	0.0456526	1.1102073	0.7771451
CD	0.0050143	0.2745381	-2.1904151	-0.1570687	-0.4733652	-0.0216703	-0.0009320	-0.0006524
CS	-0.0002603	0.0207357	125.7758946	63.0968560	0.0404920	4.1421282	0.0031648	0.0022153
CMl	-0.0000203	0.0012766	2.4494158	0.0836177	0.0032620	0.2259507	0.0002269	0.0001589
CMm	0.1759132	2.0913376	-1284.7955285	0.0575709	-85.2760422	-0.8666373	-0.8761960	-0.6133372
CMn	0.0002348	-0.0181796	-8.9021018	0.6714757	-0.0394540	-0.1110249	-0.0028209	-0.0019746

Figure B.8: Coefficients and Stability Derivatives for Truss-Braced Wing (TBW-II) configuration for α= 2.5 deg

```
****************************************************************************************************************************************************************************************

# Name               Value       Units
Sref_            1776.1245040 Lunit^2
Cref_               9.5615000 Lunit
Bref_             189.6200000 Lunit
Xcg_                5.0931460 Lunit
Ycg_                0.0000000 Lunit
Zcg_               -4.2694610 Lunit
Mach_               0.7000000 no_unit
AoA_                3.0000000 deg
Beta_               0.0000000 deg
Rho_                0.0006000 Munit/Lunit^3
Vinf_             787.7300000 Lunit/Tunit
Roll__Rate          0.0000000 rad/Tunit
Pitch_Rate          0.0000000 rad/Tunit
Yaw___Rate          0.0000000 rad/Tunit

#
Case                 Delta    Units          CFx         CFy         CFz         CMx         CMy         CMz          CL          CD          CS         CMl         CMm         CMn
#
Base_Aero            +0.000 n/a          -0.0198928  -0.0003172   0.5174377  -0.0000564   0.2203325   0.0019242   0.5177697   0.0072150  -0.0003172   0.0000564   0.2203325  -0.0019242
Alpha                +1.000 deg          -0.0353411  -0.0002759   0.6888606   0.0000210   0.0491569  -0.0004122   0.6896478   0.0127974  -0.0002759  -0.0000210   0.0491569   0.0004122
Beta                 +1.000 deg          -0.0199772   2.6010815   0.5170162  -0.0431580 -19.6314171  -0.0255118   0.5173532  -0.0382874   2.6008094   0.0431580 -19.6314171   0.0255118
Roll__Rate           +1.000 rad/Tunit    -0.0392272   9.1227751   0.5195256  -0.0367924  -0.4197064  -0.0925307   0.5208666  -0.0119836   9.1227751   0.0367924  -0.4197064   0.0925307
Pitch_Rate           +1.000 rad/Tunit    -0.0236498  -0.0000159   0.5417066   0.0000005  -0.3063011  -0.0000052   0.5422019   0.0047334  -0.0000159  -0.0000005  -0.3063011   0.0000052
Yaw___Rate           +1.000 rad/Tunit    -0.0230903   0.5701951   0.5233225  -0.0293065   0.7736431  -0.0342682   0.5238137   0.0043299   0.5701951   0.0293065   0.7736431   0.0342682
Mach                 +0.100 no_unit      -0.0269906  -0.0000355   0.6502525   0.0000045   0.1171191  -0.0001188   0.6507739   0.0070779  -0.0000355  -0.0000045   0.1171191   0.0001188
#
#
#             Base    Derivative:
#             Aero        wrt          wrt          wrt          wrt          wrt          wrt          wrt
Coef          Total       Alpha        Beta         p            q            r            Mach         U
#              -          per          per          per          per          per          per          per
#              -          rad          rad          rad          rad          rad          M            u
#
CFx       -0.0198928  -0.8851220   -0.0048303   -0.1606398   -0.6190295   -0.0265662   -0.0709778   -0.0496844
CFy       -0.0003172   0.0023641  149.0491947   75.7993194    0.0496480    4.7401076    0.0028172    0.0019721
CFz        0.5174377   9.8218104   -0.0241492    0.0173473    3.9988150    0.0488937    1.3281481    0.9297037
CMx       -0.0000564   0.0044334   -2.4695402   -0.3052217    0.0093756   -0.2430252    0.0006089    0.0004262
CMy        0.2203325  -9.8076415 -1137.4217060  -5.3177705  -86.7740548    4.5971875   -1.0321344   -0.7224941
CMz        0.0019242  -0.1338659   -1.5719655   -0.7847800   -0.3179168   -0.3007053   -0.0204297   -0.0143008
CL         0.5177697   9.8478950   -0.0238633    0.0257308    4.0257323    0.0502170    1.3300427    0.9310299
CD         0.0072150   0.3198493   -2.6070990   -0.1595118   -0.4088994   -0.0239709   -0.0013706   -0.0009594
CS        -0.0003172   0.0023641  149.0336049   75.7993194    0.0496480    4.7401076    0.0028172    0.0019721
CMl        0.0000564  -0.0044334    2.4695402    0.3052217   -0.0093756    0.2430252   -0.0006089   -0.0004262
CMm        0.2203325  -9.8076415 -1137.4217060  -5.3177705  -86.7740548    4.5971875   -1.0321344   -0.7224941
CMn       -0.0019242   0.1338659    1.5719655    0.7847800    0.3179168    0.3007053    0.0204297    0.0143008
#
```

Figure B.9: Coefficients and Stability Derivatives for Truss-Braced Wing (TBW-II) configuration for α= 3 deg

Bibliography

[1] Pfenninger, W., "Special course on concepts for drag reduction, laminar flow control, laminarization," Tech. rep., Tech. Rep., AGARD Report, 1977.

[2] Kapania, R. K., Schetz, J. A., Durham, F. D., Mallik, W., Segee, M. C., and Gupta, R., "Multidisciplinary Design Optimization and Cruise Mach Number Study of Truss-Braced Wing Aircraft," Tech. rep., NASA, 2018.

[3] Ting, E., Reynolds, K. W., Nguyen, N. T., and Totah, J., "Aerodynamic Analysis of the Truss-Braced Wing Aircraft Using Vortex-Lattice Superposition Approach," *32nd AIAA Applied Aerodynamics Conference*, 2014, p. 2597.

[4] Mason, W. H., "6. Aerodynamics of 3D Lifting Surfaces through Vortex Lattice Methods," , 1998. URL http://www.dept.aoe.vt.edu/~mason/Mason_f/CAtxtChap6.pdf.

[5] Chaparro, D., Fujiwara, G. E., Ting, E., and Nguyen, N. T., "Aerodynamic Modeling of Transonic Aircraft Using Vortex Lattice Coupled with Transonic Small Disturbance for Conceptual Design," *34th AIAA Applied Aerodynamics Conference*, 2016, p. 3418.

[6] United States Department of Transportation, "Airline Fuel Cost and Consumption," , 2022. URL https://www.transtats.bts.gov/fuel.asp.

[7] Bhatia, M., Kapania, R., van Hoek, M., and Haftka, R., "Structural design of a truss braced wing: potential and challenges," *50th AIAA/ASME/ASCE/AHS/ASC Structures, Structural Dynamics, and Materials Conference 17th AIAA/ASME/AHS Adaptive Structures Conference 11th AIAA No*, 2009, p. 2147.

[8] Gur, O., Bhatia, M., Schetz, J. A., Mason, W. H., Kapania, R. K., and Mavris, D. N., "Design optimization of a truss-braced-wing transonic transport aircraft," *Journal of aircraft*, Vol. 47, No. 6, 2010, pp. 1907–1917.

[9] Gur, O., Bhatia, M., Mason, W. H., Schetz, J. A., Kapania, R. K., and Nam, T., "Development of a framework for truss-braced wing conceptual MDO," *Structural and Multidisciplinary optimization*, Vol. 44, No. 2, 2011, pp. 277–298.

[10] Mallik, W., Kapania, R. K., and Schetz, J. A., "Effect of flutter on the multidisciplinary design optimization of truss-braced-wing aircraft," *Journal of Aircraft*, Vol. 52, No. 6, 2015, pp. 1858–1872.

[11] Gur, O., Schetz, J. A., and Mason, W. H., "Aerodynamic considerations in the design of truss-braced-wing aircraft," *Journal of Aircraft*, Vol. 48, No. 3, 2011, pp. 919–939.

[12] Gupta, R., Mallik, W., Kapania, R. K., and Schetz, J. A., "Multidisciplinary design optimization of subsonic strut-braced wing aircraft," *52nd Aerospace Sciences Meeting*, 2014, p. 0186.

[13] Mallik, W., Kapania, R. K., and Schetz, J. A., "Multidisciplinary design optimization of medium-range transonic truss-braced wing aircraft with flutter constraint," *54th AIAA/ASME/ASCE/AHS/ASC Structures, Structural Dynamics, and Materials Conference*, 2013, p. 1454.

[14] Gupta, R., Love, N. J., Kapania, R. K., and Schmidt, D., "Development of Longitudinal Flight Dynamics Analysis Framework with Controllability and Observability Metrics," *2018 Multidisciplinary Analysis and Optimization Conference*, 2018, p. 3425.

[15] McDonald, R. A., and Gloudemans, J. R., "Open Vehicle Sketch Pad: An Open

Source Parametric Geometry and Analysis Tool for Conceptual Aircraft Design," *AIAA SCITECH 2022 Forum*, 2022, p. 0004.

[16] ModelCenter 14.1 Manual, "Pheonix Integration," , 2020.

[17] Khan, K. H., Mallik, W., Kapania, R. K., and Schetz, J. A., "Distributed Design Optimization of Large Aspect Ratio Wing Aircraft with Rapid Transonic Flutter Analysis in Linux," *AIAA Scitech 2021 Forum*, 2021, p. 1354.

[18] Grasmeyer, J., "Multidisciplinary design optimization of a transonic strut-braced wing aircraft," *37th Aerospace Sciences Meeting and Exhibit*, 1999, p. 10.

[19] Gundlach IV, J. F., Tetrault, P.-A., Gern, F. H., Nagshineh-Pour, A. H., Ko, A., Schetz, J. A., Mason, W. H., Kapania, R. K., Mason, W. H., Grossman, B., et al., "Conceptual design studies of a strut-braced wing transonic transport," *Journal of Aircraft*, Vol. 37, No. 6, 2000, pp. 976–983.

[20] Meadows, N. A., Schetz, J. A., Kapania, R. K., Bhatia, M., and Seber, G., "Multidisciplinary design optimization of medium-range transonic truss-braced wing transport aircraft," *Journal of Aircraft*, Vol. 49, No. 6, 2012, pp. 1844–1856.

[21] Mallik, W., Kapania, R. K., and Schetz, J. A., "Transonic aeroelastic analysis for multidisciplinary design optimization applications," *57th AIAA/ASCE/AHS/ASC Structures, Structural Dynamics, and Materials Conference*, 2016, p. 0237.

[22] Gupta, R., Zhao, W., Kapania, R. K., and Schmidt, D. K., "Incorporating Flight Dynamics and Control Criteria into MDAO of Composite Aircraft," *AIAA Scitech 2020 Forum*, 2020, p. 1966.

[23] Ting, E., Chaparro, D., and Nguyen, N. T., "Development of an Integrated Nonlinear Aeroservoelastic Flight Dynamic Model of the Truss-Braced Wing Aircraft," *58th*

AIAA/ASCE/AHS/ASC Structures, Structural Dynamics, and Materials Conference, 2017, p. 1815.

[24] Mallik, W., "Aeroelastic Analysis of Truss-Braced Wing Aircraft: Applications for Multidisciplinary Design Optimization," Ph.D. thesis, Virginia Tech, 2016.

[25] Mariën, F., "Software Testing: VSPAERO," , 2021.

[26] Litherland, B. L., "Guides to VSPAero," , 2019. URL http://openvsp.org/wiki/doku.php?id=vspaerosummary.

[27] Abbott, I. H., and Von Doenhoff, A. E., *Theory of wing sections: including a summary of airfoil data*, Courier Corporation, 2012.

[28] Stahara, S. S., "Operational manual for two-dimensional transonic code TSFOIL," Tech. rep., NASA, 1978.